iScience

CellPress
OPEN ACCESS

Article

Maelstrom functions in the production of Siwi-piRISC capable of regulating transposons in *Bombyx* germ cells

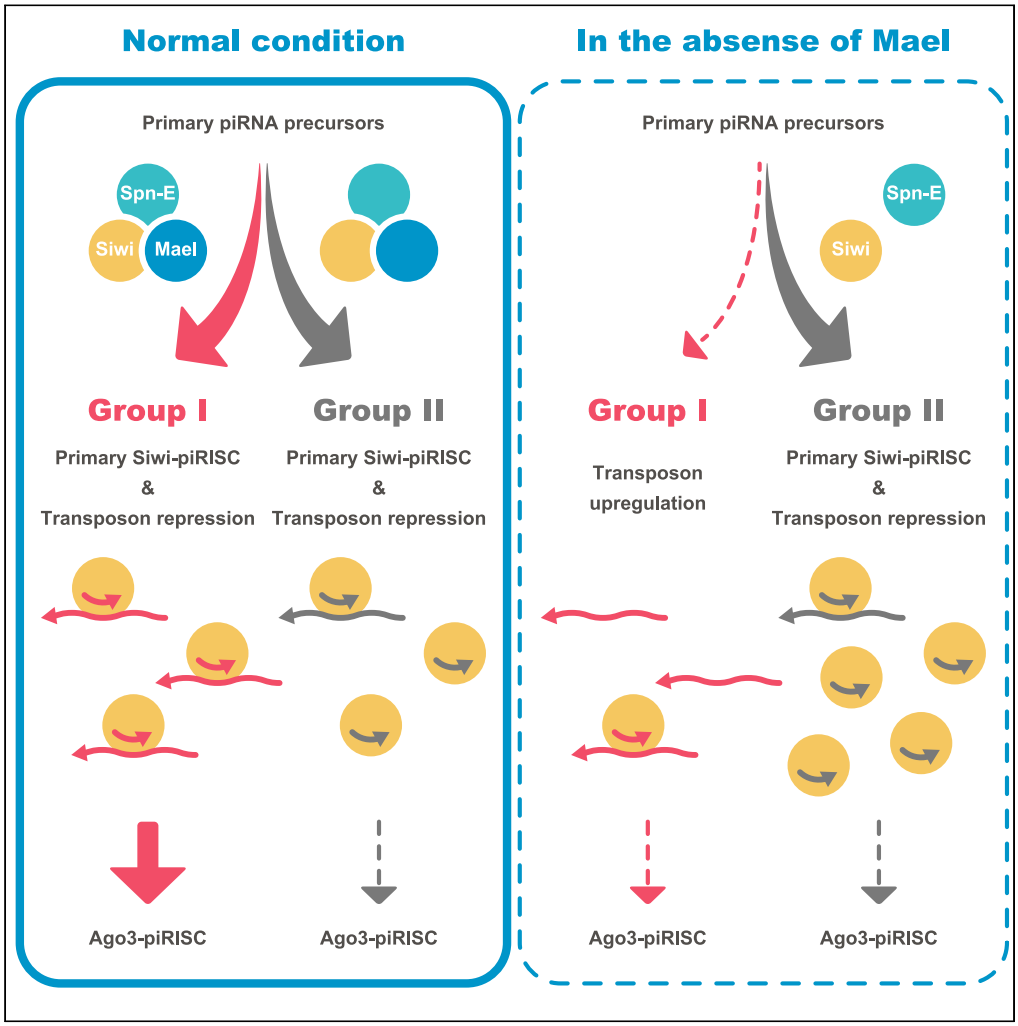

Yurika Namba, Yuka W. Iwasaki, Kazumichi M. Nishida, Hidenori Nishihara, Tetsutaro Sumiyoshi, Mikiko C. Siomi

siomim@bs.s.u-tokyo.ac.jp

Highlights

Mael interconnects Spn-E with unloaded Siwi in the Siwi-piRISC biogenesis pathway

Loss of Mael prevents Spn-E from generating Siwi-piRISC for Group I transposons

Siwi-piRISC for Group II transposons is generated, but its silencing effect is low

This explains the low level of Ago3-piRISC in Mael-lacking germ cells

Namba et al., iScience *25*, 103914
March 18, 2022
https://doi.org/10.1016/j.isci.2022.103914

iScience

CellPress
OPEN ACCESS

Article

Maelstrom functions in the production of Siwi-piRISC capable of regulating transposons in *Bombyx* germ cells

Yurika Namba,[1] Yuka W. Iwasaki,[2,3] Kazumichi M. Nishida,[1] Hidenori Nishihara,[4] Tetsutaro Sumiyoshi,[1] and Mikiko C. Siomi[1,5,*]

SUMMARY

PIWI-interacting RNAs (piRNAs) bind to PIWI proteins to assemble the piRISC, which represses germline transposons. Maelstrom (Mael) is necessary for piRISC biogenesis in germ cells, but its function remains unclear. Here, we show that Mael interconnects Spindle-E (Spn-E), a key piRISC biogenesis factor, with unloaded Siwi, one of two silkworm PIWI members. Mael also assembles a subset of nuage, a non-membranous organelle involved in piRISC biogenesis. Loss of Mael abrogated the Spn-E–Siwi interaction and Ago3-piRISC biogenesis, but Siwi-piRISC was produced. Bioinformatic analysis showed that Siwi-bound piRNAs in Mael-lacking cells were rich in transposon-targeting piRNAs as in normal cells but were biased toward transposons that are marginally controlled by Siwi-piRISC. This explains the impairment in Ago3-piRISC production because transposon mRNAs cleaved by Siwi are the origin of Ago3-loaded piRNAs. We argue that Mael plays a role in the production of primary Siwi-piRISC capable of regulating transposon expression in germ cells.

INTRODUCTION

PIWI-interacting RNAs (piRNAs) protect the germline genome from selfish transposon invasion by repressing their expression (Czech et al., 2018; Ozata et al., 2019; Yamashiro and Siomi, 2018). piRNAs alone are unable to trigger transposon silencing but do so by assembling the piRNA-induced silencing complex (piRISC) with PIWI proteins (Aravin et al., 2003; Brennecke et al., 2007; Vagin et al., 2006). Loss of piRISC function leads to transposon derepression in the germline, causing DNA damage that can lead to severe gametogenesis defects and infertility.

PIWI proteins are conserved among animal species and are classified into two groups according to their subcellular localization upon piRISC formation: cytoplasmic PIWI members exhibit endonuclease (slicer) activity and repress transposons posttranscriptionally by cleaving their mRNAs (Gunawardane et al., 2007; Nishida et al., 2007; Saito et al., 2006). In contrast, nuclear PIWI members silence transposons by suppressing transcription in concert with multiple cofactors, including histone modifiers (Onishi et al., 2021). The silkworm (*Bombyx mori*) genome contains two *PIWI* genes, *Siwi* and *Ago3*, both of which are expressed in the germline and also in *Bombyx* ovary-derived cultured germ cells (BmN4 cells) (Kawaoka et al., 2009). Both Siwi-piRISC and Ago3-piRISC are cytoplasmic and function in posttranscriptional transposon silencing (Nishida et al., 2015; Xiol et al., 2012, 2014). This indicates that the silkworm does not have a mechanism to repress transposons transcriptionally in a piRISC-dependent manner.

Siwi-piRISC is produced through two pathways: primary and secondary (Sakakibara and Siomi, 2018). The primary pathway depends on a Tudor protein, Spindle-E (Spn-E), but does not depend on Ago3 slicer (Nishida et al., 2015, 2020). Siwi-piRISC generated through this process is called primary Siwi-piRISC. In contrast, the secondary pathway depends on Ago3 slicer, and the product is called secondary Siwi-piRISC. The generation of Ago3-piRISC depends solely on a Siwi slicer. The PIWI slicer-dependent pathways to generate Ago3-piRISC and secondary Siwi-piRISC merge to form a single molecular pathway, termed the ping-pong cycle. In this pathway, Ago3 and Siwi continuously cleave transposon transcripts in the antisense and sense directions, respectively, enabling efficient repression of transposons (Nishida et al., 2015; Xiol et al., 2012, 2014).

[1]Department of Biological Sciences, Graduate School of Science, The University of Tokyo, Tokyo 113-0032, Japan

[2]Department of Molecular Biology, Keio University School of Medicine, Tokyo 160-8582, Japan

[3]Japan Science and Technology Agency, Precursory Research for Embryonic Science and Technology, Saitama 332-0012, Japan

[4]School of Life Science and Technology, Tokyo Institute of Technology, Kanagawa 226-8501, Japan

[5]Lead contact

*Correspondence: siomim@bs.s.u-tokyo.ac.jp

https://doi.org/10.1016/j.isci.2022.103914

The current model for piRISC biogenesis in BmN4 cells posits that Spn-E funnels piRNA precursors onto nascent, unbound Siwi anchored to Papi, another Tudor protein located on the mitochondrial surface (Nishida et al., 2018). Subsequently, the endonuclease, Zucchini (Zuc) (Ipsaro et al., 2012; Nishimasu et al., 2012), which is also located on the mitochondrial surface, processes the piRNA precursor bound to Siwi, giving rise to primary Siwi-piRISC.

Siwi-piRISC then initiates cleavage of transposon mRNAs for silencing. The Siwi-piRISC-cleaved RNAs are not wasted but are used to produce Ago3-bound piRNAs. For this, Siwi-piRISC folds RNAs upon cleavage until Ago3 is ready to receive them from Siwi-piRISC. The DEAD-box RNA helicase, Vasa, senses this process and displaces RNAs from Siwi-piRISC using energy from ATP hydrolysis, facilitating the generation of Ago3-piRISC. In BmN4 cells, Siwi is detected in Vasa-positive nuage, namely, Vasa bodies (Nishida et al., 2015; Xiol et al., 2014). In *Drosophila*, Vasa associates with piRNA precursors immediately after their nuclear export to assemble Vasa bodies (Zhang et al., 2012). Based on these observations, Vasa bodies are considered the site of Ago3-piRISC biogenesis.

In turn, the Ago3-piRISC-cleaved RNAs are used to produce secondary Siwi-piRISC (Nishida et al., 2015; Xiol et al., 2012, 2014). Vasa is, however, not responsible for the displacement of RNAs from Ago3-piRISC. We recently found that this depends on another DEAD-box RNA helicase, DDX43 (Murakami et al., 2021). DDX43 interacts with Ago3-piRISC and a Tudor protein, Vreteno (Vret). Both Ago3-piRISC and Vret are required to produce secondary Siwi-piRISC and to assemble nuage, termed Ago3 bodies. Thus, Ago3 bodies are considered the site of secondary Siwi-piRISC generation (Nishida et al., 2020).

Maelstrom (Mael) exerts multiple functions in the piRNA pathway and is essential for gametogenesis (Aravin et al., 2009; Castañeda et al., 2014; Lim et al., 2009; Matsumoto et al., 2015; Sienski et al., 2012; Soper et al., 2008). In *Drosophila* ovarian somatic cells, Mael is not required for piRISC biogenesis but is essential for piRNA-mediated transcriptional repression of transposons (Klenov et al., 2011; Onishi et al., 2020; Saito et al., 2010; Sienski et al., 2012). Furthermore, Mael represses canonical transcription both by piRNA and piRNA-independent mechanisms (Chang et al., 2019). Mael in adult mouse testes interacts with chromatin-remodeling factors, such as Sin3B and SNF5 (Costa et al., 2006), indicating that Mael in mice also functions in transcriptional silencing.

Mael in fetal mouse testes is detected in nuage, and loss of function of Mael abrogates secondary piRISC generation (Aravin et al., 2009). In germ cells of *Drosophila* ovaries, Mael is also detected in nuage (Findley et al., 2003; Lim and Kai, 2007; Minakhina et al., 2014; Sienski et al., 2012). *mael* mutant ovaries show defects in piRISC accumulation, thereby leading to transposon activation (Lim and Kai, 2007). However, the function of Mael in piRISC production in ovarian germ cells remains vague.

In this study, using cultured BmN4 germ cells, we show that Mael interconnects Spn-E and unloaded Siwi. Mael also assembles Mael bodies, which are physically and functionally distinguishable from other nuage, Ago3 bodies, and Vasa bodies. Loss of Mael caused loss of the Spn-E–Siwi interaction, Mael body assembly, and Ago3-piRISC biogenesis, but primary Siwi-piRISC was still produced. This indicates that the contributions of Mael and Spn-E to the production of primary Siwi-piRISC differ from each other, and that formation of Mael bodies and the Mael-dependent Spn-E–Siwi interaction are not absolutely necessary for the production of primary Siwi-piRISC. However, genome-wide sequencing of Siwi-bound primary piRNAs in Mael-deficient cells revealed that piRNAs produced in the absence of Mael are biased toward transposons that are marginally regulated by Siwi-piRISC. We propose that Mael plays a role in the generation of primary Siwi-piRISC that substantially control transposon expression in germ cells while interconnecting Spn-E and unloaded Siwi, leading to the production of Ago3-piRISC and secondary Siwi-piRISC.

RESULTS

Mael interconnects unbound Siwi with two Tudor proteins, Spn-E and Qin

To explore Mael function in piRISC biogenesis in BmN4 germ cells, we produced a monoclonal antibody against *Bombyx* Mael (Figure S1A). Immunoprecipitation using the antibody showed that Mael interacts with three proteins in BmN4 cells, whose apparent sizes were 210, 160, and 90 kDa (Figure 1A). Mass spectrometry identified them as two Tudor proteins, Qin and Spn-E, and Siwi, respectively. Western blotting corroborated their presence within the Mael complex (Figure 1B). We previously showed that Spn-E in BmN4 cells interacts with Qin and unbound Siwi (Nishida et al., 2015). We therefore hypothesized that

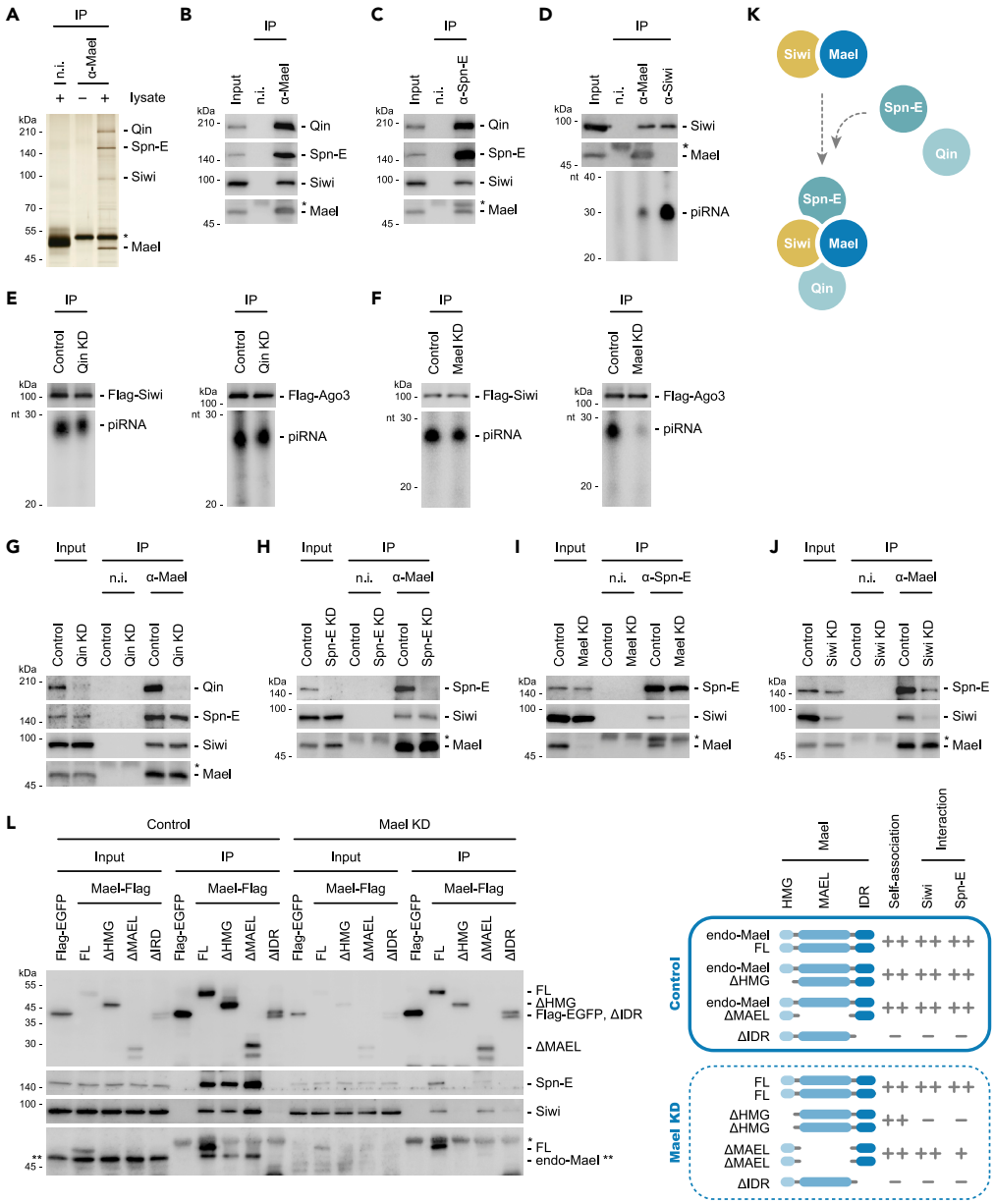

Figure 1. Mael interconnects unbound Siwi with two Tudor proteins, Spn-E and Qin

(A) Silver staining shows that Mael co-immunoprecipitated with Qin, Spn-E, and Siwi from BmN4 cell lysates. IP was performed with (+) or without (–) BmN4 cell lysates.

(B) Western blotting confirms the presence of Qin, Spn-E, Siwi, and Mael in the Mael complex in (A).

(C) Western blotting shows the presence of Qin, Spn-E, Siwi, and Mael in the Spn-E complex.

(D) The Mael complex and Siwi immunopurified from BmN4 cells were probed with anti-Siwi (top) and anti-Mael (middle) antibodies. Bottom: RNAs isolated from the two immunoprecipitates were ^{32}P-labeled.

(E) piRNAs loaded onto Flag-Siwi and Flag-Ago3 in Qin KD cells. Top: western blotting shows Flag-Siwi and Flag-Ago3 in the immunoprecipitates. Bottom: ^{32}P-labeling shows the abundance of piRNAs bound to Flag-Siwi and Flag-Ago3.

(F) piRNAs loaded onto Flag-Siwi and Flag-Ago3 in Mael KD cells. Top: western blotting shows Flag-Siwi and Flag-Ago3 in the immunoprecipitates. Bottom: ^{32}P-labeling shows the abundance of piRNAs bound to Flag-Siwi and Flag-Ago3.

(G) IP/western blotting shows that Mael remains bound with Spn-E and Siwi after Qin KD.

(H) IP/western blotting shows that Mael remains bound with Siwi after Spn-E KD.

(I) IP/western blotting shows that Spn-E did not bind to Siwi after Mael KD.

(J) IP/western blotting shows that Mael only weakly bound Spn-E after Siwi KD.

(K) Model of Mael complex assembly in BmN4 cells.

Figure 1. *Continued*
(L) Left: IP/western blotting shows that Mael ΔHMG and ΔMAEL, but not ΔIDR, mutants bound to Spn-E and Siwi in control cells similar to Mael FL. Endogenous Mael (**) was also observed within Mael FL, ΔHMG, and ΔMAEL complexes. Upon endogenous Mael KD, Mael FL is still bound to Spn-E and Siwi. Mael ΔHMG and ΔIDR mutants failed to bind Spn-E and Siwi. Mael ΔMAEL mutant bound to Siwi as efficiently as Mael FL, whereas Spn-E was barely detected. Right: data summary.
n.i.: non-immune immunoglobulin G (IgG). *: IgG heavy chain. Control: Luc KD. Flag-EGFP: negative control. See also Figure S1.

Mael may exist in the Spn-E complex and found that this was indeed the case (Figure 1C). The amount of piRNAs in the Mael complex was negligible and comparable to that in the Spn-E complex (Nishida et al., 2015) (Figure 1D). These findings indicate that the Mael complex is equivalent to the Spn-E complex and is composed of Mael, Spn-E, Qin, and unloaded Siwi.

Loss of Spn-E abandons the production of both Siwi-piRISC and Ago3-piRISC (Nishida et al., 2015). To explore the requirement of Qin and Mael in piRISC production in BmN4 cells, we expressed Flag-Siwi and Flag-Ago3 following Qin and Mael depletion and examined the levels of piRNAs loaded onto each PIWI. piRNAs were found with both PIWIs in the absence of Qin as in control cells (Figures 1E and S1B). Major piRNAs in BmN4 cells, whose expression levels were reduced by the loss of Spn-E (Nishida et al., 2015), were expressed at normal levels in Qin-depleted cells (Figure S1C). We therefore inferred that Qin may be dispensable for piRISC biogenesis in BmN4 cells. Conversely, piRNAs were loaded onto Siwi but hardly onto Ago3 in Mael-lacking cells (Figures 1F and S1D), implying that Mael is required for Ago3-piRISC but not primary Siwi-piRISC production.

To understand the interdependence of the factors that form the Mael complex, immunoprecipitation was conducted after depletion of each factor. Even following Qin depletion, Mael interacted with Spn-E and Siwi as in normal cells (Figure 1G). Thus, Qin is dispensable for the formation of a trimeric complex composed of Mael, Spn-E, and Siwi. When Spn-E was depleted, Mael bound to Siwi (Figure 1H). However, when Mael was depleted, the Siwi–Spn-E interaction was lost (Figure 1I). The interaction between Mael and Spn-E was attenuated by the loss of Siwi (Figure 1J). These results support a model in which Mael first binds unloaded Siwi and this heterodimer then interacts with Spn-E and Qin (Figure 1K).

Mael interacts with Siwi and Spn-E via the HMG box and the interaction is enhanced by Mael self-association via the C-terminal IDR

Mael consists of a high-mobility group (HMG) box, a MAEL domain (Zhang et al., 2008), and an intrinsic disordered region (IDR) (Figures S1E and S1F). The IDR has low amino acid sequence complexity and is known to be involved in the protein assembly and formation of biomolecular condensates (Banani et al., 2017). To understand how each domain of Mael is involved in the interaction with Siwi and Spn-E, we produced RNAi-resistant Mael mutants, ΔHMG, ΔMAEL, and ΔIDR, which lack the HMG, MAEL, and IDR domains, respectively, and examined their ability to interact with Spn-E and Siwi *in vivo*. In normal cells, where endogenous Mael is present, both the ΔHMG and ΔMAEL mutants interacted with Spn-E and Siwi similarly to full-length Mael (Mael FL) (Figure 1L). Endogenous Mael was also detected with Mael FL and ΔHMG and ΔMAEL mutants but not with the ΔIDR mutant. This indicates that Mael self-interacts through the IDR and that self-interaction plays a key role in the interaction of Mael with Siwi and Spn-E.

When these experiments were performed after endogenous Mael depletion, Mael FL interacted with Spn-E and Siwi as in normal cells; however, the ΔHMG mutant did not (Figure 1L). In contrast, the ΔMAEL mutant interacted well with Siwi, like Mael FL, but poorly with Spn-E. These findings further indicate that the HMG box is responsible for the interaction between Mael and Siwi, but that the Mael–Spn-E interaction via Siwi is supported by the central MAEL domain (Figure S1G).

Mael assembles Mael bodies, a subset of nuage to which Spn-E, Qin, and Siwi are localized

In BmN4 cells, Spn-E and Qin co-localize to a nuage that is distinguishable from Vasa bodies (Nishida et al., 2015). Here, we performed immunofluorescence to determine whether Mael localizes to Qin/Spn-E-positive nuage. Using a single anti-Mael antibody, Mael was shown to accumulate in perinuclear nuage-like structures (Figure 2A). Mael has an IDR at its C-terminal region (Figure S1F), and the observation that

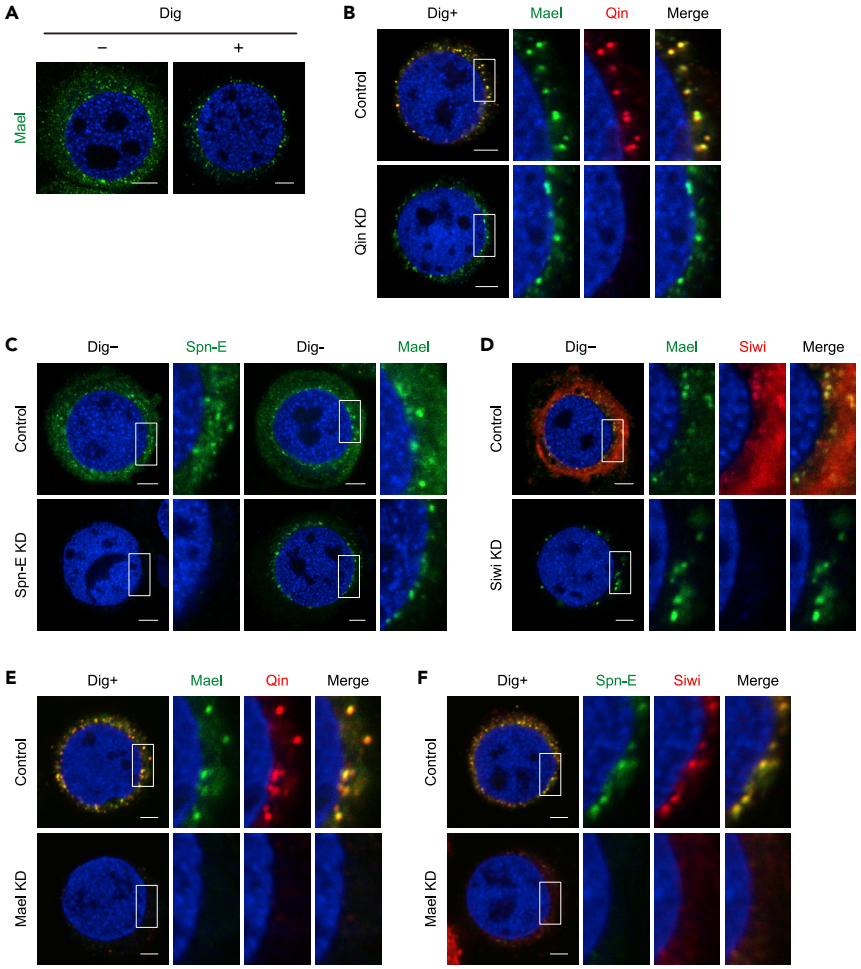

Figure 2. Mael assembles Mael bodies, a subset of nuage to which Spn-E, Qin, and Siwi are localized

(A) Subcellular localization of Mael (green) in BmN4 cells treated with (+) and without (–) Dig.

(B) Perinuclear Mael-positive bodies (Mael bodies) were present in Qin KD cells (Dig+). Green: Mael. Red: Qin.

(C) Mael bodies remain in Spn-E KD cells (Dig–). Green: Mael or Spn-E.

(D) Mael bodies remain in Siwi KD cells (Dig–). Green: Mael. Red: Siwi.

(E) Mael bodies disappeared from Mael KD cells (Dig+). In the cells, Qin failed to localize to any dot-like structures. Green: Mael. Red: Qin.

(F) In the absence of Mael bodies (Mael KD) as in (E), Spn-E and Siwi failed to localize to any dot-like structures. Green: Spn-E. Red: Siwi.

Scale bar: 5 μm. Blue (DAPI): nuclei. Control: Luc KD. See also Figure S2.

this domain acted as a self-association domain (Figures 1L and S1G) fits well with this. Furthermore, cytosolic signals of Mael were observed. However, when the cells were treated with digitonin, a nonionic solvent that permeabilizes the plasma membrane but not the nuclear membrane, and then fixed, the cytoplasmic signals almost disappeared but the Mael granules remained (Figure 2A). Because this digitonin-plus procedure produced clear Mael granular signals, it was employed for further immunostaining analyses, unless otherwise noted. We confirmed that Spn-E/Qin-positive and Siwi-positive nuage were digitonin resistant (Figure S2A).

The isotype of the anti-Spn-E antibody was identical to that of the anti-Mael antibody. Therefore, we conducted double immunostaining with anti-Mael and anti-Qin antibodies. The Mael and Qin signals almost overlapped (Figure 2B), indicating that Mael is resident in Spn-E/Qin-positive nuage. The trimeric complex containing Mael, Spn-E, and Siwi was formed in a Qin-independent manner (Figure 1G). Therefore, we hypothesized that Mael granules may be formed independently of Qin. Indeed, even when Qin

was depleted, Mael granules were detected (Figure 2B). Furthermore, the appearance of the Mael granules was little affected by the loss of Spn-E or Siwi (Figures 2C, 2D, and S2B). In contrast, the Qin, Spn-E, and Siwi granules disappeared following Mael depletion (Figures 2E and 2F). The abundance of these three proteins was hardly changed by the loss of Mael (Figure S2C). This circumstantial evidence supports Mael being the key factor in the assembly of Spn-E/Qin-positive nuage, which we hereinafter refer to as Mael bodies.

The formation of Mael bodies depends on the formation of Vasa bodies and Ago3 bodies

Nuage in BmN4 cells can be classified into Mael bodies, Vasa bodies, and Ago3 bodies according to their constituents and functions (Nishida et al., 2015, 2020; Xiol et al., 2014). To investigate the interdependency of their formation, we first assessed the dependency between Mael bodies and Vasa bodies. Remarkably, Vasa bodies were sensitive to digitonin treatment (Figure 3A); therefore, immunofluorescence was conducted without digitonin. In normal cells, Mael bodies and Vasa bodies partially overlapped with each other [Figure 3B; 33.1% (co-localization), N = 254 (granules), n = 6 (cells)]. However, immunoprecipitation/western blotting showed that the Mael complex was devoid of Vasa (Figure S3A). This result supports the interpretation that Mael bodies and Vasa bodies are practically physically separated. The apparent overlap of the two bodies may be because of the large number of bodies. It could also mean the occasional crosstalk of the two bodies.

Even when Mael was depleted, Vasa bodies were observed to be similar to those in normal cells (Figure 3B). Furthermore, Flag-Vasa was able to assemble Vasa bodies even in Mael-lacking cells (Figure 3C). These findings indicate that the assembly of Vasa bodies is independent of Mael. Conversely, when Vasa was depleted, the signal of Mael bodies was severely weakened (Figure 3D), and the disappearance of Mael bodies was not because of the reduction in the level of Mael in Vasa-lacking BmN4 cells (Figure S3B). Thus, the formation of Vasa bodies is independent of the formation of Mael bodies but not vice versa.

We next explored the interdependence of Mael bodies and Ago3 bodies in the assembly. To this end, we conducted immunofluorescence under conditions where Mael or Vret was depleted. For this, anti-Vret antibody was used to detect Ago3 bodies because Vret is a reliable marker of Ago3 bodies (Nishida et al., 2020). Ago3 bodies were resistant to digitonin (Figure S3C) and were detected to be partially overlapped with Mael bodies in normal cells, similar to Vasa bodies [Figure 3E; 48.5% (co-localization), N = 182 (granules), n = 6 (cells)]. However, like Vasa, Ago3 and Vret were not found in the Mael complex (Figure S3A). Thus, the situation of Ago3 bodies with Mael bodies is similar to that of Vasa bodies with Mael bodies.

Ago3 bodies were detected in Mael-depleted cells (Figure 3E). However, Myc-Vret expressed in Mael-depleted cells failed to assemble Ago3 bodies (Figures 3F and S3D). These results indicate that preexisting endogenous Ago3 bodies are not disrupted upon the loss of Mael, although Ago3 bodies are not newly assembled in cells lacking Mael. This is consistent with the observations that piRNAs were not loaded onto Flag-Ago3 in Mael-depleted cells (Figure 1F) and that Vret and Ago3-piRISC are necessary for Ago3 body formation (Nishida et al., 2020). Mael bodies were not detected following Vret depletion (Figures 3G and S3E). Thus, the formation of Ago3 bodies and of Mael bodies depends on each other.

Together, these findings support the notion that in BmN4 cells, Vasa body formation, which is entirely dependent on Vasa, is the highest level of nuage formation, whereas the formation of Mael bodies occurs downstream with the formation of Ago3 bodies (Figure S3F). This situation may be similar to that in *Drosophila*, where nuage is completely lost in the ovaries of *vasa* mutants (Findley et al., 2003; Pek et al., 2009).

The formation of Mael bodies is not mandatory for primary Siwi-piRISC biogenesis

The levels of Mael, Spn-E, Qin, and Siwi in BmN4 cells were hardly impacted by Vasa and Vret depletion (Figures 3H and 3I). Strikingly, all four proteins interacted with each other even upon Vret or Vasa depletion when no Mael bodies were found. This means that the formation of Mael bodies depends on Vasa and Vret, but that formation of the Mael complex is independent of Vasa and Vret. The production of primary Siwi-piRISC was hardly affected by the loss of Vasa and Vret (Nishida et al., 2015, 2020). This indicates that Mael bodies do not need to be assembled for the production of primary Siwi-piRISC.

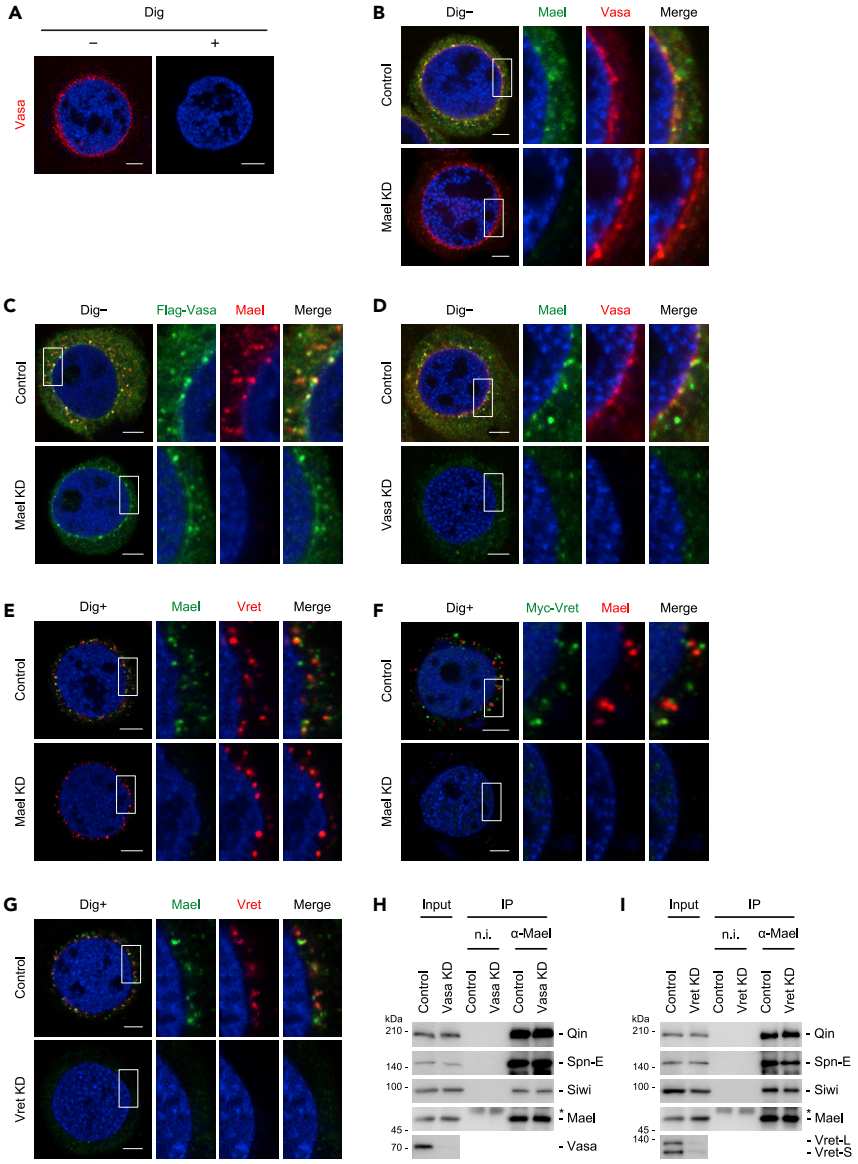

Figure 3. The formation of Mael bodies is not mandatory for primary Siwi-piRISC biogenesis

(A) Subcellular localization of Vasa (red) in BmN4 cells treated with (+) and without (–) Dig.

(B) Vasa bodies remain in Mael KD cells (Dig–). Green: Mael. Red: Vasa.

(C) Flag-Vasa assembled Vasa bodies in Mael KD cells (Dig–). Green: Flag-Vasa. Red: Mael.

(D) Mael body formation was severely attenuated in Vasa KD cells (Dig–). Green: Mael. Red: Vasa.

(E) Ago3 bodies remain in Mael KD cells (Dig+). Green: Mael. Red: Vret (an Ago3 body component).

(F) Myc-Vret failed to assemble Ago3 bodies in Mael KD cells (Dig+). Green: Myc-Vret. Red: Mael.

(G) Mael bodies were hardly assembled in Vret KD cells (Dig+). Green: Mael. Red: Vret.

(H) IP/western blotting shows that Mael binds to Qin, Spn-E, and Siwi in Vasa KD cells.

(I) IP/western blotting shows that Mael binds to Qin, Spn-E, and Siwi in Vret KD cells.

Scale bar: 5 μm. Blue (DAPI): nuclei. Control: Luc KD. n.i.: nonimmune IgG. *: IgG heavy chain. See also Figure S3.

Spn-E, but not Mael, is required for the production of primary Siwi-piRISC (Nishida et al., 2015) (Figure 1F). In the absence of Mael, Spn-E did not localize to any speckles in BmN4 cells (Figure 2F), indicating that primary Siwi-piRISC production is not a reaction that occurs within nuage or other nuage-type structures, but one that takes place at the mitochondrial surface in a Zuc-dependent manner while Siwi is anchored by Papi (Nishida et al., 2018).

Mael bodies and P-bodies are separable structures

In mouse fetal gonocytes, Mael, together with TDRD9, a mouse Spn-E homolog, and a mouse PIWI protein, MIWI2, were localized to a subset of nuage (Aravin et al., 2009). Whether a mouse Qin homolog, TDRD4, was within the granules remains unknown. The nuage were termed piP-bodies because immunofluorescent analysis showed that they frequently overlapped with processing bodies (P-bodies), which are storage chambers for some mRNAs (Decker and Parker, 2012; Luo et al., 2018). We expressed Flag-tagged Dcp1, a highly conserved resident of P-bodies, in BmN4 cells and performed immunofluorescence analysis with an anti-Mael antibody. In contrast to piP-bodies in mice, the dot-like signals of Flag-Dcp1 and Mael hardly overlapped [Figure S3G; 15.4% (co-localization), N = 140 (granules), n = 6 (cells)]. Dcp1 interacted with Me31B, another resident of P-bodies, but not with the constituent proteins of Mael bodies under the same conditions (Figure S3H). The residents of Vasa bodies and Ago3 bodies were also not included in the Dcp1 complex (Figure S3H), indicating that both Ago3 bodies and Vasa bodies could be separated from P-bodies (Figure S3G). From these results, we argue that in BmN4 cells, Mael bodies and P-bodies are separable structures. Thus, the piP-bodies in mouse germ cells (i.e., gonocytes) and Mael bodies in *Bombyx* germ cells (i.e., BmN4 cells) are similar in appearance and share some protein components, but they are not identical.

The loss of Mael and the loss of Ago3 have distinct effects on the primary Siwi-piRNA population

Mael depletion significantly reduced the level of Ago3-piRISC; however, the amount of Siwi-piRISC was hardly affected (Figure 1F). This indicates that the effect of Mael loss on piRISC production in BmN4 cells may be similar to that of Ago3 loss (Nishida et al., 2015). However, Mael, but not Ago3, binds to Spn-E (Figure S3A), albeit in an indirect fashion via unloaded Siwi (Figure 1J), and Spn-E is central to piRISC biogenesis in BmN4 cells (Nishida et al., 2015). Therefore, we hypothesized that the impact of Mael loss on Siwi-piRISC biogenesis might be different from that of Ago3 loss. To investigate this, we performed deep sequencing of piRNAs loaded onto Flag-Siwi in control cells and cells lacking Mael or Ago3 (Figure S4A). We collected sequencing reads that could be mapped to the silkworm genome (Kawamoto et al., 2019) and further mapped to a new transposon library defined in this study (i.e., 1,716 transposon sequences; see method details section). We also performed RNA sequencing (RNA-seq) of BmN4 cells before and after the loss of Siwi to analyze the effect of Siwi loss on transposon expression levels (Figure S4B). A comprehensive analysis of sequence reads in these libraries determined 211 transposons as the targets of Siwi-piRISC (Table S1); the requirement was to have more than 100 antisense Siwi-piRNA reads per million mapped reads (RPM) in one of the three small RNA libraries and 0.5 transposon reads per kilobase of transcript per million mapped reads (RPKM) in the RNA library generated from Siwi-depleted cells.

We then classified the 211 transposons into two groups by fold change (FC) and false discovery rate (FDR) of mapped piRNAs upon Ago3 depletion (Figure S4C); namely, transposons whose piRNA targeting was significantly reduced by Ago3 depletion (purple) (FC < 0 and FDR <0.01) and transposons whose piRNA targeting was not significantly reduced by Ago3 depletion (light purple) (FC ≥ 0 or FDR ≥ 0.01). We then examined how these piRNA pools were affected by the loss of Mael. The effects of Mael depletion were not significantly different in the two groups (Figure 4A). We next classified the 211 transposons by FC and FDR of mapped piRNAs upon Mael depletion (Figure S4D); namely, transposons whose piRNA targeting was reduced by Mael depletion (blue) (FC < 0 and FDR <0.01) and transposons whose piRNA targeting was barely reduced by Mael depletion (light blue) (FC ≥ 0 or FDR ≥ 0.01). There was no significant difference in the effect of Ago3 depletion on the two groups (Figure 4B). These results support the idea that primary Siwi-piRNA populations observed upon Mael or Ago3 depletion are different from each other and are likely to be independently regulated. We previously performed a similar analysis for Ago3 and Vret, which is one of the factors involved in the generation of secondary Siwi-piRISC through the ping-pong cycle (Nishida et al., 2020). In that case, the effects of Ago3 and Vret depletion on Siwi-piRNA populations were almost identical. This observation supports our hypothesis that the requirements of Ago3 and Mael in Siwi-piRISC biogenesis are different.

In parallel, we explored whether the loss of Mael affects other properties of piRNAs mapped on the silkworm genome (Kawamoto et al., 2019). First, we compared the length of Siwi-piRNAs in control cells and cells lacking Mael or Ago3. This revealed that most Siwi-piRNAs were apparently one nucleotide longer when Mael was depleted (Figure S4E). This effect was not observed when Ago3 was absent. The nucleotide bias toward uracil at the 5′ end of Siwi-piRNAs (i.e., 1U) observed in normal cells was maintained even in Mael-lacking cells as in Ago3-lacking and control cells (Figure S4F). This strongly suggests that the nucleotide addition observed in Siwi-piRNAs in Mael-lacking cells is most likely occurring at the 3′ end.

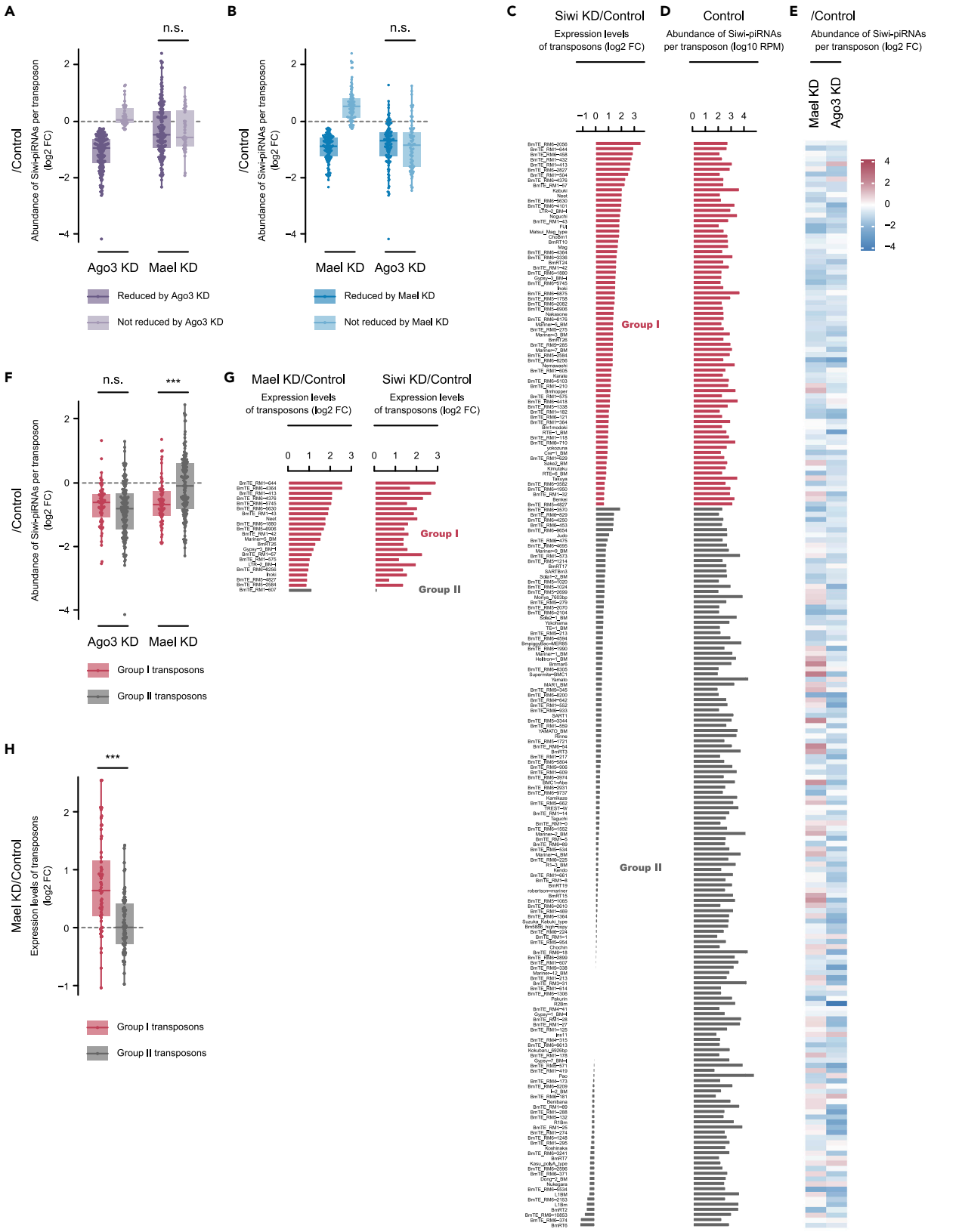
A
n.s.
/Control
Abundance of Siwi-piRNAs per transposon (log2 FC)
Ago3 KD
Mael KD
Reduced by Ago3 KD
Not reduced by Ago3 KD
B
n.s.
/Control
Abundance of Siwi-piRNAs per transposon (log2 FC)
Mael KD
Ago3 KD
Reduced by Mael KD
Not reduced by Mael KD
C
Siwi KD/Control
Expression levels of transposons (log2 FC)
Group I
Group II
D
Control
Abundance of Siwi-piRNAs per transposon (log10 RPM)
E
/Control
Abundance of Siwi-piRNAs per transposon (log2 FC)
Mael KD
Ago3 KD
F
n.s.
***
/Control
Abundance of Siwi-piRNAs per transposon (log2 FC)
Ago3 KD
Mael KD
Group I transposons
Group II transposons
G
Mael KD/Control
Expression levels of transposons (log2 FC)
Siwi KD/Control
Expression levels of transposons (log2 FC)
Group I
Group II
H
***
Mael KD/Control
Expression levels of transposons (log2 FC)
Group I transposons
Group II transposons

Figure 4. Mael plays a role in increasing the level of primary Siwi-piRISC capable of silencing transposons

(A) Boxplots show FC in the abundance of antisense Siwi-piRNAs per transposon of Ago3 and Mael KD cells relative to controls (211 transposons with over 100 antisense Siwi-piRNA RPM in one of the three small RNA libraries and with over 0.5 transposon RPKM in the Siwi KD RNA library). Each group was categorized into "Siwi-piRNAs per transposon reduced by Ago3 KD (purple, 169 transposons) (FC < 0 and FDR <0.01)" or "Siwi-piRNAs per transposon not reduced by Ago3 KD (light purple, 42 transposons) (FC ≥ 0 or FDR ≥0.01)". The effects of Mael KD (right) were not significantly different between the two groups.

(B) Boxplots show FC in the abundance of antisense Siwi-piRNAs per transposon of Mael and Ago3 KD cells relative to controls as in (A). Each group was categorized into "Siwi-piRNAs per transposon reduced by Mael KD (blue, 122 transposons) (FC < 0 and FDR <0.01)" or "Siwi-piRNAs per transposon not reduced by Mael KD (light blue, 89 transposons) (FC ≥ 0 or FDR ≥0.01)". The effects of Ago3 KD (right) were not significantly different between the two groups.

(C) The bar graph shows FC in the expression levels of transposons of Siwi KD cells relative to controls. The transposons were categorized into "Group I (red, 71 transposons) (FC > 0 and FDR <0.01)" or "Group II (gray, 140 transposons) (FC ≤ 0 or FDR ≥0.01)" and then arranged respectively by FC in descending order.

(D) The bar graph shows the abundance of antisense Siwi-piRNAs per transposon of control cells. The transposons were categorized and then arranged in (C).

(E) The heatmap shows FC in the abundance of antisense Siwi-piRNAs per transposon of Mael and Ago3 KD cells relative to controls. The transposons were categorized and then arranged in (C).

(F) Boxplots show FC in the abundance of antisense Siwi-piRNAs per transposon of Mael and Ago3 KD cells relative to controls. Group I (red) and Group II (gray) were categorized in (C).

(G) The bar graphs show FC in the expression levels of transposons of Mael (left) and Siwi (right) KD cells relative to controls. 22 transposons that were derepressed by Mael loss were categorized into Group I (21 transposons) and Group II (1 transposon) as in (C) and arranged respectively by FC in the expression levels of transposons of Mael KD cells relative to controls in descending order.

(H) Boxplots show FC in the expression levels of transposons of Mael KD cells relative to controls. 122 transposons that are potential targets of Mael-dependent piRNAs were categorized into Group I (56 transposons) and Group II (66 transposons) as in (C).

Control: Luc KD. Center line: median. Box limits: upper and lower quartiles. Whiskers: 1.5 × IQR. Points: outliers. n.s.: not significant and ***: $p < 0.001$ from Brunner-Munzel test. See also Figures S4–S6 and Tables S1 and S2.

Next, we performed a β-elimination experiment to examine whether piRNAs are modified by methyl groups at the 3′ end, as originally shown in *Drosophila* ovaries (Vagin et al., 2006). This indicates that Siwi-piRNAs generated in the absence of Mael were modified as in control cells (Nishida et al., 2018) (Figure S4G). We infer that Siwi-piRISC in Mael-lacking cells appeared to be almost fully functional despite a single nucleotide extension of the 3′ end. Finally, annotation of Siwi-piRNAs to the silkworm genome revealed that the ratio of piRNAs mapping to transposons was not much influenced by Mael depletion (Figure S4H). These findings suggest that the depletion of Mael did not significantly impact the characteristics and functionality of Siwi-piRISC.

Mael plays a role in increasing the level of primary Siwi-piRISC capable of silencing transposons

Because of the observed difference in the Siwi-bound piRNA pools in Mael-depleted and Ago3-depleted cells (Figures 4A and 4B), we inferred that the influence of Siwi-bound piRNA pools in Mael-depleted and Ago3-depleted cells on the expression of transposons under control of Siwi would also differ between Mael-depleted and Ago3-depleted conditions. To test this, we first analyzed the effect of Siwi loss on the expression level of each of the 211 transposons (i.e., the Siwi-piRISC targets) (Figure S4B). This revealed that 71 of the 211 transposons were significantly derepressed upon Siwi depletion (FC > 0 and FDR <0.01), suggesting that they are functional targets of Siwi-piRISC-dependent transposon silencing (Group I in Figures 4C and S5A). In contrast, the remaining 140 transposons were not much affected by the loss of Siwi (FC ≤ 0 or FDR ≥0.01) (Group II in Figures 4C and S5A). The levels of Siwi-piRNAs against Group I and Group II transposons in normal cells were not much different (Figure 4D), verifying that both are potential targets of Siwi-piRISC.

We then overlaid this with the FC of piRNAs targeting each transposon upon Mael or Ago3 depletion. This revealed that, in the case of Mael depletion, piRNAs mapped to transposons tended to be decreased specifically for those mapped to Group I transposons (i.e., transposons actively controlled by Siwi-piRISC), whereas piRNAs mapped to Group II transposons (i.e., transposons marginally controlled by Siwi-piRISC) remained unchanged or increased (Figure 4E). In contrast, loss of Ago3 reduced the number of piRNAs that targeted most of the transposons in an unbiased manner (Figures 4E and S5B). Statistical analysis of piRNA pools mapped to Group I and Group II transposons illustrated the difference between Mael and Ago3 depletion (Figure 4F); namely, the significant difference was observed only in Mael-lacking cells. These results suggest that Mael plays a role in the generation of primary Siwi-piRISC that regulates the expression of transposons substantially via targeting.

We performed RNA-seq in Mael-lacking BmN4 cells (Figure S4B). Our earlier analysis estimated that 122 of 211 transposons (i.e., the Siwi-piRISC targets) are potential targets of Mael-dependent piRNAs (57.8%) (Figures 4B and S4D). The RNA-seq reads in Mael-depleted cells showed that 22 of the 122 transposons were significantly derepressed by Mael loss (18.0%) (Figure S5C). Remarkably, 21 of the 22 transposons belonged to Group I (95.5%) (Figures 4G and S5C). Statistical analysis revealed that Group I transposons tended to be more affected by the loss of Mael than Group II transposons (Figures 4H and S5C), and this result showed a positive correlation with the result shown in Figure 4F. Based on these findings, we argued that Mael plays a role in increasing the level of Siwi-piRISC that practically silences Group I transposons in the germ cells.

Group I transposons are evolutionarily younger than group II transposons

A recent study showed that most piRNAs target evolutionally younger transposons in mammalian germlines (Ishino et al., 2021). We thus considered the possibility that Group I transposons are relatively younger than Group II transposons. It is known that younger transposons do not accumulate mutations as older transposons do (Lander et al., 2001). Therefore, we curated each Group I and Group II transposon, determined the copy number in the silkworm genome (Kawamoto et al., 2019), and examined the degree of sequence divergence from the consensus sequence of the transposon library (Table S2). The Group I transposons were found to have a lower copy number and less sequence divergence than the Group II transposons (Figure S6A). This supports the idea that Group I transposons are relatively younger. This outcome seems to agree with the above observation that the expression levels of Group I transposons are actively regulated by Siwi more than Group II transposons. Moreover, the obvious differences in the ages and contents of LINE families between Group I and Group II suggest the possibility that young copies of LINE families such as L2 clade LINEs in the genome might have transposed recently and primary Siwi-piRISC distinctively regulates their activity (Figure S6B). These results provide another possibility for Group II transposons to escape regulation by Siwi-piRISC; whereas we based our analysis on the silkworm reference genome (Kawamoto et al., 2019), the BmN4 genome used in this study has accumulated sequence divergences of evolutionarily older Group II transposons, the piRNAs targeting of which may reduce the efficiency of silencing.

DISCUSSION

In this study, we found that Mael plays a role in increasing the level of primary Siwi-piRISC, which effectively represses Group I transposons in normal BmN4 cells (Figure 5). The level of Siwi-piRISC was not low in Mael-deficient BmN4 cells, but the piRNAs within Siwi-piRISC were biased toward transposons that are virtually unaffected by the loss of Siwi (i.e., Group II transposons). Group I and Group II transposons were derepressed by the loss of Siwi, but the effect was much weaker for Group II transposons. This implies that mRNAs of Group II transposons are less likely to be targets of Siwi-mediated cleavage. Siwi-cleaved RNAs are the sole origin of piRNAs loaded onto Ago3; under such circumstances (without Mael), the level of Ago3-piRISC is inevitably low. In Mael-lacking cells, Vasa bodies were present, but Siwi was not localized very efficiently to the bodies. This observation also explains that piRNAs within Siwi-piRISC were biased toward Group II transposons; the target RNAs are abundant, but the amount of Siwi that targets them is low (Figure 5).

How then does Mael maintain the level of Siwi-piRISC that represses Group I transposons in BmN4 cells? In this study, two properties of Mael were revealed. That is, Mael interconnects unloaded Siwi with Spn-E (along with Qin), and Mael assembles Mael bodies to which Spn-E, Qin, and Siwi are localized. We initially thought that Mael bodies might contribute to the function of Mael to increase the level of primary Siwi-piRISC to regulate Group I transposons. However, we found that this was not the case based on the observation that in the absence of Vret and Vasa, Mael bodies were not assembled, but Siwi-piRISC was still produced. The loss of Vret and Vasa did not have a strong impact on primary Siwi-piRISC biogenesis (Nishida et al., 2015, 2020). However, in the absence of Vret and Vasa, the Mael complex was still formed. Therefore, we inferred that this function of Mael, that is, interconnecting Spn-E with unloaded Siwi, may be the key in maintaining the level of Siwi-piRISC against Group I transposons (Figure 5).

In Spn-E-deficient cells, the production of primary Siwi-piRISC is nearly totally attenuated (Nishida et al., 2015); therefore, Spn-E is central for piRISC biogenesis in BmN4 cells. Spn-E has one Tudor domain and one DExH-box RNA helicase domain (Gillespie and Berg, 1995). It is envisioned that Spn-E binds piRNA precursors transcribed from piRNA clusters and actively funnels them to unbound Siwi anchored on the surface of mitochondrial via Papi, and that this function of Spn-E is supported by Mael. It is possible that piRNA precursors that generate

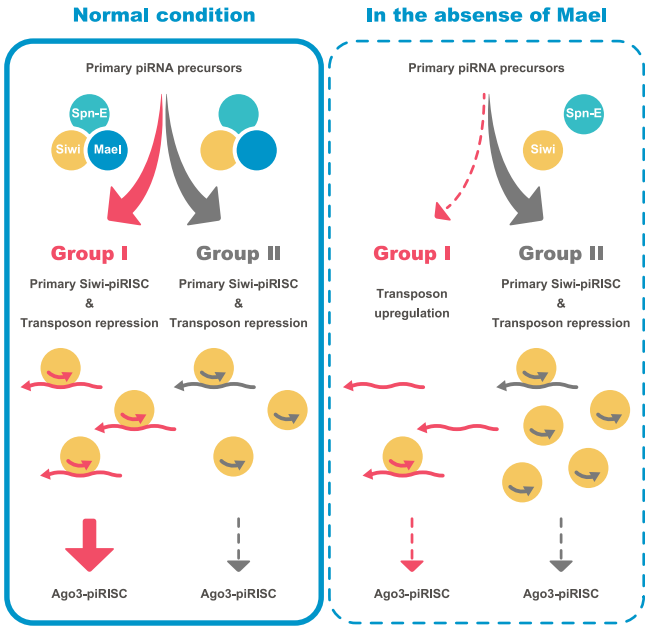

Figure 5. Model of Siwi-piRISC biogenesis and transposon repression in BmN4 germ cells

In normal BmN4 cells (left), Mael interconnects Spn-E and unloaded Siwi, ensuring the production of Siwi-piRISC to silence both Group I and Group II transposons. Group I transposons tend to be younger with a lower copy number and less sequence divergence than Group II transposons, suggesting that Group I transposons are more efficient at transposition and piRNAs can silence Group I transposons efficiently than Group II transposons with accumulated mutations. Therefore, when those mRNAs are cleaved in a Siwi-dependent manner, Ago3-piRISC is generated based on Group I mRNAs rather than Group II mRNAs. In Mael-depleted BmN4 cells (right), where Mael only weakly interconnects Spn-E with unloaded Siwi, mRNAs of Group I transposons are still abundantly produced, but Siwi-piRISC targeting Group I transposons is rarely produced while Siwi-piRISC targeting Group II transposons is produced normally, reducing the level of Ago3-piRISC biogenesis.

piRNAs against Group I and Group II transposons have differences in families or some unique features in silkworms, and that Mael encourages Spn-E to actively produce piRNAs against Group I transposons by not only recognizing and distinguishing features of the precursors directly or indirectly but also interconnecting Spn-E and unloaded Siwi (Figure 5). Indeed, our curation showed that Group I transposons have a lower copy number and less sequence divergence than Group II transposons. This suggested that Group I transposons are evolutionarily younger than Group II transposons. One hypothesis is that Spn-E, in collaboration with Mael, may discern this age difference between Group I and Group II as a unique feature. The MAEL domain of Mael in *Bombyx, Drosophila,* and mice exhibits endonuclease activity *in vitro* (Chen et al., 2015; Matsumoto et al., 2015). Studies in mice also showed that the HMG box of Mael has a preference to bind double-stranded nucleic acids *in vitro*, rather than single-stranded (Genzor and Bortvin, 2015). These properties of Mael may also be used in Mael's role in supporting the function of Spn-E. At present, these are only speculations, and further investigation, such as identification and thorough analysis of the piRNA clusters, is required for providing an accurate answer to the question.

Notably, this study also contributed to the definition of the transposon library containing 1,716 transposons by analysis of the recently reported silkworm genome (Kawamoto et al., 2019). Before this study, the effect of transposon derepression by the loss of piRNA function in BmN4 cells was thought to be very weak (Izumi et al., 2013; Katsuma et al., 2020; Xiol et al., 2012). However, we noticed that the extent of transposon derepression was not so trivial in BmN4 cells (for example, see Figure 4C). This may include evolutionally younger transposons that were overlooked in previous studies.

Limitations of the study

In this study, we proposed a model for Mael function in primary Siwi-piRISC biogenesis in silkworm ovarian germ (BmN4) cells, but the details of how Mael promotes piRISC generation specifically for evolutionarily

young (Group I) transposons remain unclear. Elucidating the biological significance of Mael body assembly is also a future challenge.

STAR★METHODS

Detailed methods are provided in the online version of this paper and include the following:

- KEY RESOURCES TABLE
- RESOURCE AVAILABILITY
  - Lead contact
  - Materials availability
  - Data and code availability
- EXPERIMENTAL MODEL AND SUBJECT DETAILS
- METHOD DETAILS
  - cDNA cloning
  - Plasmid construction
  - Production of monoclonal antibodies
  - RNAi and transgene expression
  - Western blotting
  - Immunoprecipitation
  - Isolation of PIWI-associated small RNAs
  - β-elimination
  - Northern blotting
  - Sequence alignment and domain analysis
  - Immunofluorescence
  - Nuage imaging analysis
  - Identification of new transposons
  - Preparation of PIWI-associated small RNA libraries
  - Preparation of RNA libraries
  - Sequence analysis of PIWI-associated small RNA reads
  - Sequence analysis of RNA reads
  - Transposon classification
- QUANTIFICATION AND STATISTICAL ANALYSIS

SUPPLEMENTAL INFORMATION

Supplemental information can be found online at https://doi.org/10.1016/j.isci.2022.103914.

ACKNOWLEDGMENTS

We are grateful to I. Sagawa for mass spectrometry, Y. Okada for confocal microscopy, A. Nakamura for the anti-Me31B antibody, and Y. Miyata and A. Kajiya for technical assistance. We also thank H. Siomi, K. Sato, S. Hirakata, R. Onishi, H. Ishizu, H. Yamazaki, and K. Sakakibara for the discussion. This study was supported by research grants from MEXT to M.C.S. (19H05466), K.M.N. (20K06483), and Y.W.I. (21H00259). Y.N. (16J02082) and T.S. (18J11121) were supported by JSPS, and Y.W.I. was supported by JST PRESTO (JPMJPR20E2).

AUTHOR CONTRIBUTIONS

Y.N. and K.M.N. performed biochemical experiments. Y.N., Y.W.I., and T.S. performed bioinformatic analyses. Y.N. and H.N. characterized transposons computationally. M.C.S. supervised and discussed the work and wrote the manuscript with authors.

DECLARATION OF INTERESTS

The authors declare no competing interests.

Received: July 16, 2021
Revised: December 27, 2021
Accepted: February 8, 2022
Published: March 18, 2022

REFERENCES

Aravin, A.A., Lagos-Quintana, M., Yalcin, A., Zavolan, M., Marks, D., Snyder, B., Gaasterland, T., Meyer, J., and Tuschl, T. (2003). The small RNA profile during Drosophila melanogaster development. Dev. Cell *5*, 337–350.

Aravin, A.A., van der Heijden, G.W., Castañeda, J., Vagin, V.V., Hannon, G.J., and Bortvin, A. (2009). Cytoplasmic compartmentalization of the fetal piRNA pathway in mice. PLoS Genet. *5*, e1000764.

Banani, S.F., Lee, H.O., Hyman, A.A., and Rosen, M.K. (2017). Biomolecular condensates: organizers of cellular biochemistry. Nat. Rev. Mol. Cell Biol. *18*, 285–298.

Bao, W., Kojima, K.K., and Kohany, O. (2015). Repbase Update, a database of repetitive elements in eukaryotic genomes. Mob. DNA *6*, 11.

Brennecke, J., Aravin, A.A., Stark, A., Dus, M., Kellis, M., Sachidanandam, R., and Hannon, G.J. (2007). Discrete small RNA-generating loci as master regulators of transposon activity in Drosophila. Cell *128*, 1089–1103.

Brunner, E., and Munzel, U. (2000). The nonparametric Behrens-Fisher problem: asymptotic theory and a small-sample approximation. Biomed. J. *42*, 17–25.

Castañeda, J., Genzor, P., van der Heijden, G.W., Sarkeshik, A., Yates, J.R., 3rd, Ingolia, N.T., and Bortvin, A. (2014). Reduced pachytene piRNAs and translation underlie spermiogenic arrest in Maelstrom mutant mice. EMBO J. *33*, 1999–2019.

Chang, T.H., Mattei, E., Gainetdinov, I., Colpan, C., Weng, Z., and Zamore, P.D. (2019). Maelstrom represses canonical polymerase II transcription within Bi-directional piRNA clusters in Drosophila melanogaster. Mol. Cell *73*, 291–303.e6.

Chen, K.-M., Campbell, E., Pandey, R.R., Yang, Z., McCarthy, A.A., and Pillai, R.S. (2015). Metazoan Maelstrom is an RNA-binding protein that has evolved from an ancient nuclease active in protists. RNA *21*, 833–839.

Costa, Y., Speed, R.M., Gautier, P., Semple, C.A., Maratou, K., Turner, J.M.A., and Cooke, H.J. (2006). Mouse MAELSTROM: the link between meiotic silencing of unsynapsed chromatin and microRNA pathway? Hum. Mol. Genet. *15*, 2324–2334.

Czech, B., Munafò, M., Ciabrelli, F., Eastwood, E.L., Fabry, M.H., Kneuss, E., and Hannon, G.J. (2018). piRNA-guided genome defense: from biogenesis to silencing. Annu. Rev. Genet. *52*, 131–157.

Decker, C.J., and Parker, R. (2012). P-bodies and stress granules: possible roles in the control of translation and mRNA degradation. Cold Spring Harb. Perspect. Biol. *4*, a012286.

Dobin, A., Davis, C.A., Schlesinger, F., Drenkow, J., Zaleski, C., Jha, S., Batut, P., Chaisson, M., and Gingeras, T.R. (2012). STAR: ultrafast universal RNA-seq aligner. Bioinformatics *29*, 15–21.

Eddy, S.R. (2011). Accelerated profile HMM searches. PLoS Comput. Biol. *7*, e1002195.

Findley, S.D., Tamanaha, M., Clegg, N.J., and Ruohola-Baker, H. (2003). Maelstrom, a Drosophila spindle-class gene, encodes a protein that colocalizes with Vasa and RDE1/AGO1 homolog, Aubergine, in nuage. Development *130*, 859–871.

Flynn, J.M., Hubley, R., Goubert, C., Rosen, J., Clark, A.G., Feschotte, C., and Smit, A.F. (2020). RepeatModeler2 for automated genomic discovery of transposable element families. Proc. Natl. Acad. Sci. U S A *117*, 9451–9457.

Genzor, P., and Bortvin, A. (2015). A unique HMG-box domain of mouse Maelstrom binds structured RNA but not double stranded DNA. PLoS One *10*, e0120268.

Gillespie, D.E., and Berg, C.A. (1995). Homeless is required for RNA localization in Drosophila oogenesis and encodes a new member of the DE-H family of RNA-dependent ATPases. Genes Dev. *9*, 2495–2508.

Gunawardane, L.S., Saito, K., Nishida, K.M., Miyoshi, K., Kawamura, Y., Nagami, T., Siomi, H., and Siomi, M.C. (2007). A slicer-mediated mechanism for repeat-associated siRNA 5′ end formation in Drosophila. Science *315*, 1587–1590.

Ipsaro, J.J., Haase, A.D., Knott, S.R., Joshua-Tor, L., and Hannon, G.J. (2012). The structural biochemistry of Zucchini implicates it as a nuclease in piRNA biogenesis. Nature *491*, 279–283.

Ishino, K., Hasuwa, H., Yoshimura, J., Iwasaki, Y.W., Nishihara, H., Seki, N.M., Hirano, T., Tsuchiya, M., Ishizaki, H., Masuda, H., et al. (2021). Hamster PIWI proteins bind to piRNAs with stage-specific size variations during oocyte maturation. Nucleic Acids Res. *49*, 2700–2720.

Izumi, N., Kawaoka, S., Yasuhara, S., Suzuki, Y., Sugano, S., Katsuma, S., and Tomari, Y. (2013). Hsp90 facilitates accurate loading of precursor piRNAs into PIWI proteins. RNA *19*, 896–901.

Jones, D.T., and Cozzetto, D. (2015). DISOPRED3: precise disordered region predictions with annotated protein-binding activity. Bioinformatics *31*, 857–863.

Kapitonov, V.V., Tempel, S., and Jurka, J. (2009). Simple and fast classification of non-LTR retrotransposons based on phylogeny of their RT domain protein sequences. Gene *448*, 207–213.

Katsuma, S., Shoji, K., Suzuki, Y., and Kiuchi, T. (2020). CRISPR/Cas9-mediated mutagenesis of Ago2 and Siwi in silkworm cultured cells. Gene, 145314.

Kawamoto, M., Jouraku, A., Toyoda, A., Yokoi, K., Minakuchi, Y., Katsuma, S., Fujiyama, A., Kiuchi, T., Yamamoto, K., and Shimada, T. (2019). High-quality genome assembly of the silkworm, Bombyx mori. Insect Biochem. Mol. Biol. *107*, 53–62.

Kawaoka, S., Hayashi, N., Suzuki, Y., Abe, H., Sugano, S., Tomari, Y., Shimada, T., and Katsuma, S. (2009). The Bombyx ovary-derived cell line endogenously expresses PIWI/PIWI-interacting RNA complexes. RNA *15*, 1258–1264.

Klenov, M.S., Sokolova, O.A., Yakushev, E.Y., Stolyarenko, A.D., Mikhaleva, E.A., Lavrov, S.A., and Gvozdev, V.A. (2011). Separation of stem cell maintenance and transposon silencing functions of Piwi protein. Proc. Natl. Acad. Sci. U S A *108*, 18760–18765.

Kohany, O., Gentles, A.J., Hankus, L., and Jurka, J. (2006). Annotation, submission and screening of repetitive elements in Repbase: RepbaseSubmitter and Censor. BMC Bioinformatics *7*, 474.

Lander, E.S., Linton, L.M., Birren, B., Nusbaum, C., Zody, M.C., Baldwin, J., Devon, K., Dewar, K., Doyle, M., FitzHugh, W., et al. (2001). Initial sequencing and analysis of the human genome. Nature *409*, 860–921.

Langmead, B., Trapnell, C., Pop, M., and Salzberg, S.L. (2009). Ultrafast and memory-efficient alignment of short DNA sequences to the human genome. Genome Biol. *10*, R25.

Li, H., Handsaker, B., Wysoker, A., Fennell, T., Ruan, J., Homer, N., Marth, G., Abecasis, G., Durbin, R., and 1000 Genome Project Data Processing Subgroup. (2009). The sequence alignment/map format and SAMtools. Bioinformatics *25*, 2078–2079.

Lim, A.K., and Kai, T. (2007). Unique germ-line organelle, nuage, functions to repress selfish genetic elements in Drosophila melanogaster. Proc. Natl. Acad. Sci. U S A *104*, 6714–6719.

Lim, A.K., Tao, L., and Kai, T. (2009). piRNAs mediate posttranscriptional retroelement silencing and localization to pi-bodies in the Drosophila germline. J. Cell Biol. *186*, 333–342.

Lu, S., Wang, J., Chitsaz, F., Derbyshire, M.K., Geer, R.C., Gonzales, N.R., Gwadz, M., Hurwitz, D.I., Marchler, G.H., Song, J.S., et al. (2020). CDD/SPARCLE: the conserved domain database in 2020. Nucleic Acids Res. *48*, D265–D268.

Luo, Y., Na, Z., and Slavoff, S.A. (2018). P-bodies: composition, properties, and functions. Biochemistry *57*, 2424–2431.

Martin, M. (2011). Cutadapt removes adapter sequences from high-throughput sequencing reads. EMBnet.Journal *17*, 10–12.

Matsumoto, N., Sato, K., Nishimasu, H., Namba, Y., Miyakubi, K., Dohmae, N., Ishitani, R., Siomi, H., Siomi, M.C., and Nureki, O. (2015). Crystal structure and activity of the endoribonuclease domain of the piRNA pathway factor maelstrom. Cell Rep. *11*, 366–375.

Minakhina, S., Changela, N., and Steward, R. (2014). Zfrp8/PDCD2 is required in ovarian stem cells and interacts with the piRNA pathway machinery. Development *141*, 259–268.

Murakami, R., Sumiyoshi, T., Negishi, L., and Siomi, M.C. (2021). DEAD-box polypeptide 43 facilitates piRNA amplification by actively liberating RNA from Ago3-piRISC. EMBO Rep. *22*, e51313.

Nakamura, A., Amikura, R., Hanyu, K., and Kobayashi, S. (2001). Me31B silences translation of oocyte-localizing RNAs through the formation

of cytoplasmic RNP complex during Drosophila oogenesis. Development *128*, 3233–3242.

Nishida, K.M., Saito, K., Mori, T., Kawamura, Y., Nagami-Okada, T., Inagaki, S., Siomi, H., and Siomi, M.C. (2007). Gene silencing mechanisms mediated by Aubergine–piRNA complexes in Drosophila male gonad. RNA *13*, 1911–1922.

Nishida, K.M., Iwasaki, Y.W., Murota, Y., Nagao, A., Mannen, T., Kato, Y., Siomi, H., and Siomi, M.C. (2015). Respective functions of two distinct Siwi complexes assembled during PIWI-interacting RNA biogenesis in Bombyx germ cells. Cell Rep. *10*, 193–203.

Nishida, K.M., Sakakibara, K., Iwasaki, Y.W., Yamada, H., Murakami, R., Murota, Y., Kawamura, T., Kodama, T., Siomi, H., and Siomi, M.C. (2018). Hierarchical roles of mitochondrial Papi and Zucchini in Bombyx germline piRNA biogenesis. Nature *555*, 260–264.

Nishida, K.M., Sakakibara, K., Sumiyoshi, T., Yamazaki, H., Mannen, T., Kawamura, T., Kodama, T., and Siomi, M.C. (2020). Siwi levels reversibly regulate secondary pi RISC biogenesis by affecting Ago3 body morphology in Bombyx mori. EMBO J. *39*, e105130.

Nishimasu, H., Ishizu, H., Saito, K., Fukuhara, S., Kamatani, M.K., Bonnefond, L., Matsumoto, N., Nishizawa, T., Nakanaga, K., Aoki, J., et al. (2012). Structure and function of Zucchini endoribonuclease in piRNA biogenesis. Nature *491*, 284–287.

Onishi, M., Yamano, K., Sato, M., Matsuda, N., and Okamoto, K. (2021). Molecular mechanisms and physiological functions of mitophagy. EMBO J. *40*, e104705.

Onishi, R., Sato, K., Murano, K., Negishi, L., Siomi, H., and Siomi, M.C. (2020). Piwi suppresses transcription of Brahma-dependent transposons via Maelstrom in ovarian somatic cells. Sci. Adv. *6*, eaaz7420.

Ou, S., and Jiang, N. (2018). LTR_retriever: a highly accurate and sensitive program for identification of long terminal repeat retrotransposons. Plant Physiol. *176*, 1410–1422.

Ozata, D.M., Gainetdinov, I., Zoch, A., O'Carroll, D., and Zamore, P.D. (2019). PIWI-interacting RNAs: small RNAs with big functions. Nat. Rev. Genet. *20*, 89–108.

Pek, J.W., Lim, A.K., and Kai, T. (2009). Drosophila maelstrom ensures proper germline stem cell lineage differentiation by repressing microRNA-7. Dev. Cell *17*, 417–424.

Quinlan, A.R., and Hall, I.M. (2010). BEDTools: a flexible suite of utilities for comparing genomic features. Bioinformatics *26*, 841–842.

R Core Team (2020). R: A Language and Environment for Statistical Computing (The R Development Core Team).

Robinson, M.D., McCarthy, D.J., and Smyth, G.K. (2010). edgeR: a Bioconductor package for differential expression analysis of digital gene expression data. Bioinformatics *26*, 139–140.

Saito, K., Nishida, K.M., Mori, T., Kawamura, Y., Miyoshi, K., Nagami, T., Siomi, H., and Siomi, M.C. (2006). Specific association of Piwi with rasiRNAs derived from retrotransposon and heterochromatic regions in the Drosophila genome. Genes Dev. *20*, 2214–2222.

Saito, K., Ishizu, H., Komai, M., Kotani, H., Kawamura, Y., Nishida, K.M., Siomi, H., and Siomi, M.C. (2010). Roles for the Yb body components Armitage and Yb in primary piRNA biogenesis in Drosophila. Genes Dev. *24*, 2493–2498.

Sakakibara, K., and Siomi, M.C. (2018). The PIWI-interacting RNA molecular pathway: insights from cultured silkworm germline cells. Bioessays *40*, 1700068.

Schindelin, J., Arganda-Carreras, I., Frise, E., Kaynig, V., Longair, M., Pietzsch, T., Preibisch, S., Rueden, C., Saalfeld, S., Schmid, B., et al. (2012). Fiji: an open-source platform for biological-image analysis. Nat. Methods *9*, 676–682.

Schneider, C.A., Rasband, W.S., and Eliceiri, K.W. (2012). NIH Image to ImageJ: 25 years of image analysis. Nat. Methods *9*, 671–675.

Sienski, G., Dönertas, D., and Brennecke, J. (2012). Transcriptional silencing of transposons by Piwi and maelstrom and its impact on chromatin state and gene expression. Cell *151*, 964–980.

Smit, A.F.A., Hubley, R., and Green, P. (2015). RepeatMasker Open-4.0. 2013–2015 (ISB).

Song, L., and Florea, L. (2015). Rcorrector: efficient and accurate error correction for Illumina RNA-seq reads. Gigascience *4*, 48.

Soper, S.F.C., van der Heijden, G.W., Hardiman, T.C., Goodheart, M., Martin, S.L., de Boer, P., and Bortvin, A. (2008). Mouse maelstrom, a component of nuage, is essential for spermatogenesis and transposon repression in meiosis. Dev. Cell *15*, 285–297.

Storer, J., Hubley, R., Rosen, J., Wheeler, T.J., and Smit, A.F. (2021). The Dfam community resource of transposable element families, sequence models, and genome annotations. Mob. DNA *12*, 2.

Vagin, V.V., Sigova, A., Li, C., Seitz, H., Gvozdev, V., and Zamore, P.D. (2006). A distinct small RNA pathway silences selfish genetic elements in the germline. Science *313*, 320–324.

Xiol, J., Cora, E., Koglgruber, R., Chuma, S., Subramanian, S., Hosokawa, M., Reuter, M., Yang, Z., Berninger, P., Palencia, A., et al. (2012). A role for Fkbp6 and the chaperone machinery in piRNA amplification and transposon silencing. Mol. Cell *47*, 970–979.

Xiol, J., Spinelli, P., Laussmann, M.A., Homolka, D., Yang, Z., Cora, E., Couté, Y., Conn, S., Kadlec, J., Sachidanandam, R., et al. (2014). RNA clamping by Vasa assembles a piRNA amplifier complex on transposon transcripts. Cell *157*, 1698–1711.

Yamashiro, H., and Siomi, M.C. (2018). PIWI-interacting RNA in Drosophila: biogenesis, transposon regulation, and beyond. Chem. Rev. *118*, 4404–4421.

Zhang, D., Xiong, H., Shan, J., Xia, X., and Trudeau, V.L. (2008). Functional insight into Maelstrom in the germline piRNA pathway: a unique domain homologous to the DnaQ-H 3'–5'exonuclease, its lineage-specific expansion/loss and evolutionarily active site switch. Biol. Direct *3*, 48.

Zhang, F., Wang, J., Xu, J., Zhang, Z., Koppetsch, B.S., Schultz, N., Vreven, T., Meignin, C., Davis, I., Zamore, P.D., et al. (2012). UAP56 couples piRNA clusters to the perinuclear transposon silencing machinery. Cell *151*, 871–884.

STAR★METHODS

KEY RESOURCES TABLE

REAGENT or RESOURCE	SOURCE	IDENTIFIER
Antibodies		
anti-Mael mouse monoclonal	This study	6G8
anti-Mael mouse monoclonal	This study	6B11
anti-Siwi mouse monoclonal	(Nishida et al., 2015)	30E2
anti-Spn-E mouse monoclonal	(Nishida et al., 2015)	7B2E10
anti-Qin mouse monoclonal	(Nishida et al., 2015)	1D1F8
anti-Vasa mouse monoclonal	(Nishida et al., 2015)	1C3D10
anti-Vasa mouse monoclonal	(Nishida et al., 2015)	3B11B10
anti-Vret mouse monoclonal	(Nishida et al., 2020)	9G6
anti-Ago3 mouse monoclonal	(Nishida et al., 2015)	7A7
anti-Me31B rabbit polyclonal	(Nakamura et al., 2001)	N/A
anti-β-Tubulin mouse monoclonal	Developmental Studies Hybridoma Bank	Cat#E7; RRID: AB_528499
anti-Flag M2 mouse monoclonal	Sigma-Aldrich	Cat#F3165; RRID: AB_259529
anti-Flag rabbit polyclonal	Sigma-Aldrich	Cat#F7425
anti-Myc mouse monoclonal	Developmental Studies Hybridoma Bank	Cat#9E10; RRID: AB_2266850
anti-Myc rabbit polyclonal	Sigma-Aldrich	Cat#C3956
anti-mouse IgG (H+L) HRP	Cappel	Cat#55558
anti-mouse Ig HRP TrueBlot ULTRA	Rockland	Cat#18-8817-33, RRID: AB_2610851
anti-rabbit IgG HRP-linked	Cell Signaling Technology	Cat#7074, RRID: AB_2099233
Alexa Fluor 488 goat anti-mouse IgG1	Thermo Fisher Scientific	Cat#A-21121; RRID: AB_2535764
Alexa Fluor 555 goat anti-mouse IgG1	Thermo Fisher Scientific	Cat#A-21127; RRID: AB_2535769
Alexa Fluor 555 goat anti-mouse IgG2a	Thermo Fisher Scientific	Cat#A-21137; RRID: AB_2535776
Alexa Fluor 488 goat anti-rabbit IgG	Thermo Fisher Scientific	Cat#A-11008, RRID: AB_143165
Bacterial and virus strains		
Escherichia coli Rosetta 2 (DE3)	Novagen	Cat#71397
Chemicals, peptides, and recombinant proteins		
EX-CELL 420 Serum-Free Medium for Insect cells	Sigma-Aldrich	Cat#14420C
Fetal Bovine Serum	Equitech-Bio	Cat#SFBM30-0025
Penicillin-Streptomycin-Glutamine	Gibco	Cat#10378016
SMARTer RACE 5′/3′ Kit	Clontech	Cat#634858
NEBuilder HiFi DNA Assembly Master Mix	New England Biolabs	Cat#E2621X
Glutathione Sepharose 4B	Cytiva	Cat#17-0756-01
Phosphate-buffered saline	FUJIFILM Wako Pure Chemical	Cat#048-29805
Thiophilic-Superflow Resin	Clontech	Cat#Z5616N
FuGENE HD Transfection Reagent	Promega	Cat#E2312
Nitrocellulose Membrane	FUJIFILM Wako Pure Chemical	Cat#030-25643
Immobilon-P membrane	Merck	Cat#IPVH00010
ECL Prime Western Blotting Detection Reagent	Cytiva	Cat#RPN2232
Dynabeads Protein G	Thermo Fisher Scientific	Cat#10009D
SilverQuest Silver Staining Kit	Thermo Fisher Scientific	Cat#LC6070

(*Continued on next page*)

Continued

REAGENT or RESOURCE	SOURCE	IDENTIFIER
RNasin Plus Ribonuclease Inhibitor	Promega	Cat#N2615
Proteinase K	Roche	Cat#03115828001
Antarctic Phosphatase	New England Biolabs	Cat#M0289L
T4 Polynucleotide Kinase	New England Biolabs	Cat#M0201L
ISOGEN II	FUJIFILM Wako Pure Chemical	Cat#311-07361
Hybond-N membrane	Cytiva	Cat#RPN303N
VECTASHIELD Antifade Mounting Medium with DAPI	VECTOR LABORATORIES	Cat#H-1200
Critical commercial assays		
Nucleofector 2b device	Lonza	Cat#AAB-1001
ChemiDoc XRS Plus System	Bio-Rad	Cat#1708265J1PC
NEBNext Small RNA Library Prep Set for Illumina	New England Biolabs	Cat#E7330S
VAHTS Stranded mRNA-seq Library Prep Kit for Illumina	Vazyme	Cat#NR602
Deposited data		
Raw and analyzed data	This study	GEO: GSE180191
Original images	This study	https://doi.org/10.17632/gyrjt3xfg8.1
Bombyx reference genome (Genome assembly; Nov. 2016) in SilkBase	(Kawamoto et al., 2019)	http://silkbase.ab.a.u-tokyo.ac.jp/cgi-bin/index.cgi
Bombyx transposon consensus sequences in Repbase	(Bao et al., 2015; Kohany et al., 2006)	RRID: SCR_021169, https://www.girinst.org/repbase/
Dfam	(Storer et al., 2021)	RRID: SCR_021168, https://dfam.org/home
Experimental models: Cell lines		
Bombyx ovary-derived cultured germ cells (BmN4 cells)	National Institute of Agrobiological Sciences (NIAS)	N/A
Experimental models: Organisms/strains		
Oligonucleotides		
Primer and probe sequences	Table S3	N/A
Small RNA sequences	Table S3	N/A
Recombinant DNA		
pGEX5X-GST-Mael	This study	N/A
pIB-3×Flag-EGFP	(Nishida et al., 2015)	N/A
pIB-3×Flag-Siwi	(Nishida et al., 2015)	N/A
pIB-3×Flag-Ago3	(Nishida et al., 2015)	N/A
pIB-3×Flag-Vasa	(Nishida et al., 2015)	N/A
pIB-3×Flag-Vret-L	(Nishida et al., 2020)	N/A
pIB-3×Myc-Vret-L	This study	N/A
pIB-3×Flag-Dcp1	This study	N/A
pIB-Mael-3×Flag, FL and various mutants	This study	N/A
Software and algorithms		
ImageJ	(Schneider et al., 2012)	RRID: SCR_003070; https://imagej.net/
Fiji	(Schneider et al., 2012)	RRID: SCR_002285; http://fiji.sc
DISOPRED3	(Jones and Cozzetto, 2015)	RRID: SCR_010248; http://bioinf.cs.ucl.ac.uk
RepeatModeler	(Flynn et al., 2020)	RRID: SCR_015027; http://www.repeatmasker.org/RepeatModeler/

(*Continued on next page*)

Continued

REAGENT or RESOURCE	SOURCE	IDENTIFIER
LTR_retriever	(Ou and Jiang, 2018)	RRID: SCR_017623; https://github.com/oushujun/LTR_retriever
Cutadapt	(Martin, 2011)	RRID: SCR_011841; http://code.google.com/p/cutadapt/
Bowtie	(Langmead et al., 2009)	RRID: SCR_005476; http://bowtie-bio.sourceforge.net/index.shtml
SAMtools	(Li et al., 2009)	RRID: SCR_002105; http://htslib.org/
BEDTools	(Quinlan and Hall, 2010)	RRID: SCR_006646; https://github.com/arq5x/bedtools2
RepeatMasker	(Smit et al., 2015)	RRID: SCR_012954; http://repeatmasker.org/
Rcorrector	(Song and Florea, 2015)	https://github.com/mourisl/Rcorrector
TranscriptomeAssemblyTools	N/A	https://github.com/harvardinformatics/TranscriptomeAssemblyTools
Trim Galore	N/A	RRID: SCR_011847; http://www.bioinformatics.babraham.ac.uk/projects/trim_galore/
STAR	(Dobin et al., 2012)	RRID: SCR_004463; http://code.google.com/p/rna-star/
HMMER	(Eddy, 2011)	RRID: SCR_005305; http://hmmer.janelia.org/
RTclass1	(Kapitonov et al., 2009)	https://www.girinst.org/RTphylogeny/RTclass1/
CD-search tool	(Lu et al., 2020)	RRID: SCR_018756; https://www.ncbi.nlm.nih.gov/Structure/bwrpsb/bwrpsb.cgi
R	(R Core Team, 2020)	RRID: SCR_001905; http://www.r-project.org/
edgeR	(Robinson et al., 2010)	RRID: SCR_012802; http://bioconductor.org/packages/edgeR/
Brunnermunzel	(Brunner and Munzel, 2000)	https://cran.r-project.org/web/packages/brunnermunzel/index.html

RESOURCE AVAILABILITY

Lead contact

Further information and requests for resources and reagents should be directed to and will be fulfilled by the lead contact, Mikiko C. Siomi (siomim@bs.s.u-tokyo.ac.jp).

Materials availability

Plasmids and antibodies generated in this study will be shared by the lead contact upon request.

Data and code availability

- RNA-seq data have been deposited at GEO and are publicly available as of the date of publication. The accession number is listed in the key resources table. Original images have been deposited at Mendeley and are publicly available as of the date of publication. The DOI is listed in the key resources table.
- This paper does not report original code.
- Any additional information required to reanalyze the data reported in this paper is available from the lead contact upon request.

EXPERIMENTAL MODEL AND SUBJECT DETAILS

Bombyx ovary-derived cultured germ cells (BmN4 cells) were cultured at 26 °C in EX-CELL 420 Serum-Free Medium for Insect cells (Sigma-Aldrich) supplemented with 10% Fetal Bovine Serum (FBS) (Equitech-Bio) and Penicillin-Streptomycin-Glutamine (Gibco).

METHOD DETAILS

cDNA cloning

Dcp1 cDNA was obtained by RT-PCR using total RNAs from BmN4 cells. The 5′-end of *Dcp1* mRNA was determined by 5′ RACE using the SMARTer RACE 5′/3′ Kit (Clontech). PCR primers used are summarized in Table S3.

Plasmid construction

Vectors for expressing glutathione S-transferase (GST)-Mael, Flag-Dcp1, and Mael-Flag were generated by inserting each cDNA into pGEX5X, pIB-3×Flag (N-terminal), and pIB-3×Flag (C-terminal) vectors, respectively, using NEBuilder HiFi DNA Assembly Master Mix (New England Biolabs). Vectors for expressing Myc-Vret-L and Mael-Flag mutants [ΔHMG (77–440 a.a.), ΔMAEL (1–88 and 335–440 a.a.), and ΔIDR (1–339 a.a.)] were generated by inverse PCR using vectors expressing Flag-Vret-L and Mael-Flag (FL and RNAi-resistant), respectively. PCR primers and plasmids used are summarized in Table S3 and the key resources table.

Production of monoclonal antibodies

Recombinant GST-Mael was expressed in *Escherichia coli* Rosetta 2 (DE3) (Novagen) and purified from the lysate using Glutathione Sepharose 4B (Cytiva) with Elution Buffer [0.5 M Tris-HCl (pH 8.8), 10 mM glutathione, and 10% glycerol]. The eluted fractions were collected and dialyzed against phosphate-buffered saline (PBS) (FUJIFILM Wako Pure Chemical) for three hours and then against PBS containing 10% glycerol for 18 h at 4°C. The purified antigen immunized mice every two weeks. Hybridomas were produced by fusing lymph node or spleen cells from injected mice with myeloma cells. Hybridomas were screened by enzyme-linked immuno sorbent assay (ELISA), western blotting, immunoprecipitation, and immunostaining.

RNAi and transgene expression

To deplete endogenous proteins, BmN4 cells (1×10^6) were transfected with 500 pmol of siRNA duplexes in 100 μL of EP buffer [2.1 mM HEPES-KOH (pH 7.1), 137 mM NaCl, 5 mM KCl, and 0.5 mM Na_2HPO_4] using program T-001 of the Nucleofector 2b device (Lonza). siRNA duplexes were repeatedly transfected every 5 days twice to increase the RNAi effect. After 10 days, the cells were harvested. Luciferase (Luc) siRNA was used as a control. The siRNAs used are summarized in Table S3. To exogenously express proteins, BmN4 cells (6×10^5) were transfected with 2–8 μL plasmids and 5–20 μL FuGENE HD Transfection Reagent (Promega) in 100 μL complete medium without FBS. Three hours after transfection, 10% FBS was added to the cell medium, and the cells were cultured for 2 days and harvested.

Western blotting

Protein samples for western blotting were diluted with 2× sample buffer [125 mM Tris-HCl (pH 6.8), 4% SDS, 19% glycerol, 200 mM DTT, and 0.01% bromophenol blue]. The samples were separated by sodium dodecyl sulfate polyacrylamide electrophoresis (SDS-PAGE) and then blotted onto Nitrocellulose Membrane (FUJIFILM Wako Pure Chemical) or Immobilon-P membrane (Merck). After blocking with 5% skim milk, membranes were incubated with primary antibodies in PBS containing 0.1% Tween (T-PBS) at room temperature. Anti-Mael (this study), anti-Siwi, anti-Spn-E, anti-Qin, anti-Vasa, anti-Ago3 (Nishida et al., 2015), anti-Vret (Nishida et al., 2020), anti-Me31B (Nakamura et al., 2001), anti-Flag M2 (Sigma-Aldrich), anti-β-Tubulin, and anti-Myc (Developmental Studies Hybridoma Bank) antibodies were used as primary antibodies. After washing with T-PBS, membranes were incubated with secondary antibodies in T-PBS at room temperature. Anti-mouse IgG (H+L) HRP (Cappel), anti-mouse Ig HRP TrueBlot ULTRA (Rockland), and anti-rabbit IgG HRP-linked (Cell Signaling Technology) antibodies were used as secondary antibodies. After washing with T-PBS, the membranes were then incubated with ECL Prime Western Blotting Detection Reagent (Cytiva). Images were collected using the ChemiDoc XRS Plus System (Bio-Rad).

Immunoprecipitation

Dynabeads Protein G (Thermo Fisher Scientific) and antibodies were incubated in PBS containing 0.02% Tween at room temperature. Anti-Mael (this study), anti-Siwi, anti-Spn-E, anti-Qin (Nishida et al., 2015), and anti-Flag M2 (Sigma-Aldrich) antibodies were used. BmN4 cells were lysed at 4°C with immunoprecipitation (IP) buffer [30 mM HEPES-KOH (pH 7.3), 150 mM KOAc, 2 mM $Mg(OAc)_2$, 5 mM DTT, 0.1% NP-40, 2 μg/mL pepstatin, 2 μg/mL leupeptin, and 0.5% aprotinin]. After the cell debris was removed by centrifugation, the cell lysates were incubated with antibody-conjugated beads for 1 h at 4°C. After protein–antibody binding, the beads were washed extensively with IP buffer. The immunoprecipitated proteins

were eluted with 2× sample buffer, separated by SDS-PAGE, and detected by western blotting or silver staining using SilverQuest Silver Staining Kit (Thermo Fisher Scientific).

Isolation of PIWI-associated small RNAs

Immunoprecipitation was performed as described above. To lyse BmN4 cells, IP buffer containing RNasin Plus Ribonuclease Inhibitor (Promega) was used. After protein-antibody binding, the beads were washed once with IP buffer containing 500 mM NaCl (this step was skipped to purify the Mael complexes in Figure 1D) and then extensively with IP buffer. The protein-bound RNAs were purified from the beads by proteinase K (Roche) treatment followed by phenol/chloroform treatment, and precipitated with ethanol. The 5′ ends of the RNAs were dephosphorylated with Antarctic Phosphatase (New England Biolabs) and radiolabeled with ^{32}P-γ-ATP by T4 polynucleotide kinase (New England Biolabs). After diluted with 2× gel loading buffer II (95% formamide, 18 mM EDTA, 0.025% SDS, 0.025% xylene cyanol FF, and 0.025% bromophenol blue), the RNAs were separated by denaturing (6 M urea) PAGE and detected using imaging plates and a Typhoon FLA 9500 laser scanner (Cytiva).

β-elimination

PIWI-associated small RNAs were isolated as described above. The labeled RNAs were first incubated with 10 mM $NaIO_4$ containing 5 μg yeast tRNA for 40 min at 4°C in the dark. The oxidized RNAs were then precipitated with ethanol and incubated with 1 M L (+)-Lysine-HCl (pH 8.5) for 90 min at 45°C to achieve β-elimination. After precipitated with ethanol and diluted with 2× gel loading buffer II, the RNAs were separated by denaturing (7 M urea) PAGE and detected using imaging plates and a Typhoon FLA 9500 laser scanner. The small RNA used is listed in Table S3.

Northern blotting

Total RNA was isolated from BmN4 cells using ISOGEN II (FUJIFILM Wako Pure Chemical) and 5 μg samples were separated by denaturing (7 M urea) PAGE and transferred onto Hybond-N membrane (Cytiva). After N-(3-dimethylaminopropyl)-N′-ethylcarbodiimide hydrochloride (EDC)-crosslinking, hybridization was performed at 42°C for 18 h in hybridization buffer [200 mM sodium phosphate buffer (pH 7.2), 7% SDS, and 1 mM EDTA] with end-labeled antisense DNA oligos. Membranes were then washed at 42°C in 2× saline sodium citrate and 0.1% SDS. DNA oligos used are summarized in Table S3. The blots were imaged using imaging plates and a Typhoon FLA 9500 laser scanner.

Sequence alignment and domain analysis

The amino-acid sequence of Mael was obtained from the National Center for Biotechnology Information (NCBI) database under reference sequence number: XP_037873150.1. The disorder profile was mapped via DISOPRED3 (Jones and Cozzetto, 2015).

Immunofluorescence

BmN4 cells were placed on 0.075% poly-L-lysine coated glass coverslips. The cells were treated with or without 35 μg/mL digitonin in PBS for 5 min, fixed with 4% formaldehyde in PBS for 15 min, and permeabilized with 0.1% Triton X-100 in PBS for 15 min. After blocking with 3% bovine serum albumin (BSA) in PBS, the cells were incubated with primary antibodies diluted with 3% BSA in PBS at room temperature. Anti-Mael (this study), anti-Siwi, anti-Spn-E, anti-Qin, anti-Vasa (Nishida et al., 2015), anti-Vret (Nishida et al., 2020), anti-Flag (Sigma-Aldrich), and anti-Myc (Sigma-Aldrich) antibodies were used as primary antibodies. After washing with PBS, the cells were incubated with secondary antibodies diluted in PBS with 3% BSA at room temperature in the dark. Alexa Fluor 488 goat anti-mouse IgG1, Alexa Fluor 555 goat anti-mouse IgG1, Alexa Fluor 555 goat anti-mouse IgG2a, and Alexa Fluor 488 goat anti-rabbit IgG antibodies (Thermo Fisher Scientific) were used as secondary antibodies. After washing with PBS, the cells were mounted with VECTASHIELD Antifade Mounting Medium with DAPI (VECTOR LABORATORIES). Images were collected using a Zeiss LSM980 laser-scanning microscope with a Plan-Apochromat 63×/1.4 Oil DIC objective lens. Pixel dwell time was set at 2.05 μs and two sequentially scanned images were averaged.

Nuage imaging analysis

Images of immunostaining were processed with ImageJ (Schneider et al., 2012) and Fiji (Schindelin et al., 2012). Images were split into each channel and filtered using "median" with a radius of 2 pixels. Nuage was defined using Threshold "MaxEntropy" with "Dark background" and Binary "Watershed". Using Analyze

Particles "Centroid", particles of nuage were counted and the centroid of each particle was calculated. After particle definition and centroid calculation against one cell of channel A and B, for example protein A and B, the squares of the distance between the centroids in channel A and B were calculated comprehensively. When the squares of the distance were less than 5 pixels, the two particles were defined as co-localized. The numbers of protein A/B-positive nuage were counted and the ratios were calculated.

Identification of new transposons

One hundred and six *Bombyx* transposon consensus sequences retrieved from Repbase (accessed on Feb 19, 2021) (Bao et al., 2015) were integrated with 121 *Bombyx* transposons (Kawaoka et al., 2009). Additionally, using RepeatModeler (version 2.0.1) (Flynn et al., 2020) coupled with LTR_retriever (version 2.9.0) (Ou and Jiang, 2018), 1,736 *de novo* repetitive elements (transposons) were obtained from the *Bombyx* reference genome (Genome assembly; Nov. 2016) in SilkBase (Kawamoto et al., 2019). Redundant sequences within those 1,963 transposons were discarded by a BLASTN search, resulting in 1,716 transposon sequences. We used this pool as a new transposon library in this study.

Preparation of PIWI-associated small RNA libraries

PIWI-associated small RNAs were isolated as described above. Small RNA libraries were prepared from control, Ago3 KD, and Mael KD BmN4 cells using the NEBNext Small RNA Library Prep Set for Illumina (New England Biolabs) and sequenced using the MiSeq system (Illumina) to obtain 51 nt single-end reads. A total of 5,903,981 and 2,298,981 reads were obtained from the control libraries, 3,809,418 and 3,191,812 reads were obtained from the Ago3 KD libraries, and 3,873,966 and 2,425,964 reads were obtained from the Mael KD libraries (Replicate 1 and 2, respectively).

Preparation of RNA libraries

Total RNAs were isolated using ISOGEN II and DNase (Life technologies). RNA libraries were prepared from control, Siwi KD, and Mael KD BmN4 cells using the VAHTS Stranded mRNA-seq Library Prep Kit for Illumina (Vazyme) and sequenced using the NovaSeq system (Illumina) to obtain paired-end reads. A total of 52,826,202 and 40,090,590 reads were obtained from the control libraries, 41,868,622 and 51,350,714 reads were obtained from the Ago3 KD libraries, and 55,698,164 and 45,572,492 reads were obtained from the Mael KD libraries (Replicate 1 and 2, respectively).

Sequence analysis of PIWI-associated small RNA reads

After removal of adaptor sequences by Cutadapt (version 3.1) (Martin, 2011), 22–35 nt reads were mapped to the genome using Bowtie (version 1.3.0) (Langmead et al., 2009) in random and multiple counting modes not allowing mismatch. Genome-mapped reads were processed using SAMtools (Li et al., 2009) and BEDTools (Quinlan and Hall, 2010), normalized by the number of genome-mapped reads, and then used for analyses in Figures S4A, S4E, S4F, and S4H. To determine annotation of the reads, transposon feature data were obtained from RepeatMasker (version 4.1.1) (Smit et al., 2015) using the transposon library for transposon regions, and reads were assigned to the feature when its overlap was longer than 90% of the length. The genome-mapped reads were aligned to the transposon library using Bowtie in random and multiple counting modes allowing up to two mismatches. The 211 transposons with over 100 antisense Siwi-piRNA RPM in one of the three small RNA libraries and with over 0.5 transposon RPKM in the Siwi KD RNA library (see sequence analysis of RNA reads section) were listed in Table S1 and used for analyses in Figures 4A–4H, S4C, S4D, S5A–S5C, S6A, S6B, and Table S2.

Sequence analysis of RNA reads

After cleaning and removal of adaptor sequences using Rcorrector (version 1.0.4) (Song and Florea, 2015), TranscriptomeAssemblyTools, and TrimGalore, over 36 nt reads were mapped to the genome and to the transposon library using STAR (version 2.7.9a) (Dobin et al., 2012) in random and multiple counting modes allowing up to 4% mismatches relative to read length. Genome-mapped reads were processed using SAMtools (Li et al., 2009) and BEDTools (Quinlan and Hall, 2010), normalized by the number of genome-mapped reads. The genome-mapped reads were aligned to the transposon library in the same way as above, and then used for analyses in Figure S4B. The 211 transposons with over 100 antisense Siwi-piRNA RPM in one of the three small RNA libraries (see sequence analysis of PIWI-associated small RNA reads section) and with over 0.5 transposon RPKM in the Siwi KD RNA library were listed in Table S1 and used for analyses in Figures 4A–H, S4C, S4D, S5A–S5C, S6A, S6B, and Table S2.

Transposon classification

To reidentify the repeat class and superfamily/clades of the 211 transposons, we used CENSOR to search homologous sequences of the 211 consensus sequences in eukaryotic repetitive elements in Repbase (accessed on Sep 27, 2021) (Kohany et al., 2006). This search was conducted for both the nucleotide and translated amino acid sequences. Also, a homology search was conducted using nhmmscan in HMMER (version 3.3.2) (Eddy, 2011) against the profile hidden Markov models of transposons in Dfam (release 3.4) (Storer et al., 2021). For LINE-like sequences, we used RTclass1 to further classify the clades (Kapitonov et al., 2009). For other repeats containing open reading frames, translated amino acid sequences were used for a domain search using the NCBI CD-search tool (Lu et al., 2020) to identify the transposon types. Non-coding transposons were classified based on sequence features such as promoter boxes for SINEs and terminal inverted repeats for DNA transposons. To estimate the number of transposon copies in the *Bombyx* genome, RepeatMasker (version 4.1.1) (Smit et al., 2015) was used with the custom library of 1,716 transposon sequences. The number of copies of the 211 transposons was calculated based on the RepeatMasker output for 0.5% bins of sequence divergence from each consensus sequence.

QUANTIFICATION AND STATISTICAL ANALYSIS

Experiments in Figures 1A–AJ, 1L, 2A–2F, 3A–3I, S1A–S1D, S2A–S2C, S3A–S3E, S3G, S3H, and S4G were independently performed twice with similar results. Statistical analyses were performed in the R software environment (version 4.0.3) (R Core Team, 2020). To calculate fold change (FC) and false discovery rate (FDR) in Figures 4A–4H, S4C, S4D, S5A, and S5C, the edgeR package (version 3.32.1) (Robinson et al., 2010) was used. To calculate P values from Brunner–Munzel test in Figures 4A, 4B, 4F, and 4H, the brunner-munzel package (version 1.4.1) (Brunner and Munzel, 2000) was used. P values < 0.05 were considered statistically significant and described as follows; n.s.: not significant and ***: $P < 0.001$. No statistical methods were used to predetermine sample size. The experiments were not randomized, and investigators were not blinded to allocation during experiments and outcome assessment.